A ONE-LINE NUMERICAL MODEL FOR SHORELINE EVOLUTION UNDER THE INTERACTION OF WIND WAVES AND OFFSHORE BREAKWATERS

A THESIS SUBMITTED TO
THE GRADUATE SCHOOL OF NATURAL AND APPLIED SCIENCES
OF
MIDDLE EAST TECHNICAL UNIVERSITY

BY

SALİH SERKAN ARTAGAN

IN PARTIAL FULFILLMENT OF THE REQUIREMENTS
FOR
THE DEGREE OF MASTER OF SCIENCE
IN
CIVIL ENGINEERING

JULY 2006

Approval of the Graduate School of Natural and Applied Sciences

_____
Prof.Dr. Canan Özgen
Director

I certify that this thesis satisfies all the requirements as a thesis for the degree of Master of Science.

_____

Prof.Dr. Erdal Çokça
Head of Department

This is to certify that we have read this thesis and that in our opinion it is fully adequate, in scope and quality, as a thesis for the degree of Master of Science .

_____
Dr.Işıkhan Güler
Co-Supervisor

_____
Prof.Dr. Ayşen Ergin
Supervisor

Examining Committee Members:

Assoc.Prof.Dr. Nuri Merzi	(METU, CE)	_____
Prof.Dr. Ayşen Ergin	(METU, CE)	_____
Dr. Işıkhan Güler	(METU, CE)	_____
Assoc.Prof.Dr. Ahmet Cevdet Yalçıner	(METU, CE)	_____
Assoc.Prof.Dr. Mehmet Ali Kökpınar	(DSİ)	_____

I hereby declare that all information in this document has been obtained and presented in accordance with academic rules and ethical conduct. I also declare that, as required by these rules and conduct, I have fully cited and referenced all material and results that are not original to this work.

Name, Last name : Salih Serkan, ARTAGAN

Signature :

ABSTRACT

A ONE-LINE NUMERICAL MODEL FOR SHORELINE EVOLUTION UNDER THE INTERACTION OF WIND WAVES AND OFFSHORE BREAKWATERS

ARTAGAN, Salih Serkan

M.S. Department of Civil Engineering

Supervisor: Prof.Dr. Ayşen ERGİN

Co-Supervisor: Dr. Işıkhan GÜLER

July 2006, 102 Pages

A numerical model based on one-line theory is developed to evaluate the wind wave driven longshore sediment transport rate and shoreline change. Model performs wave transformation from deep water through the surf zone and computes the breaking parameters. The formula of longshore sediment transport rate used in the numerical model is selected as a result of comparative studies with the similar expressions and the field measurements. Offshore breakwater module of the numerical model is developed to compute the change of shoreline behind single or multiple offshore breakwaters. The validity of the numerical model was confirmed by comparing model results with the shoreline change given within the sheltered zone behind the offshore

breakwaters. A series of offshore breakwaters are hypothetically proposed for a case study where a series of groins were constructed whose numerical model results qualitatively matched well with the field measurements. The results of the influences of offshore breakwaters on the shoreline predicted by the model are discussed comparatively with the case study.

Keywords: Shoreline Change, Longshore Sediment Transport, Offshore Breakwater, One-line Theory

ÖZ

RÜZGAR DALGALARI VE AÇIK DENİZ DALGAKIRANI ETKİLEŞİMİ ALTINDA KIYI ÇİZGİSİ HAREKETİ İÇİN TEK-ÇİZGİ SAYISAL MODELİ

ARTAGAN, Salih Serkan

Yüksek Lisans, İnşaat Mühendisliği Bölümü

Tez Yöneticisi: Prof.Dr. Ayşen ERGİN

Ortak Tez Yöneticisi: Dr. Işıkhan GÜLER

Temmuz 2006, 102 Sayfa

Rüzgar dalgalarının neden olduğu kıyı boyu katı madde taşınımını ve kıyı çizgisi değişimini değerlendirmek için tek-çizgi teorisi temel alınarak sayısal bir model geliştirilmiştir. Model, rüzgar dalgalarının derin denizden kırılma bölgesine kadar olan transformasyonunu vermekte ve kırılma parametrelerini hesaplamaktadır. Sayısal modelde kullanılan kıyı boyu katı madde taşınımı denklemi benzer denklemlerle ve saha ölçümleriyle yapılan karşılaştırmalı çalışma sonucu seçilmiştir. Tek ya da birden çok açık deniz dalgakıranının arkasındaki kıyı çizgisi değişimini hesaplamak için sayısal programın açık deniz dalgakıran modulü geliştirilmiştir. Sayısal modelin geçerliliği model sonuçlarının açık deniz dalgakıranının arkasında

korunan alandaki kıyı çizgisi değişimi ile kıyaslanarak gösterilmiştir. Saha ölçümü ile model sonuçları nitelik olarak uyum gösteren seri mahmuzların yapılmış olduğu bir uygulamada seri açık deniz dalgakıranları hipotetik olarak önerilmiştir. Açık deniz dalgakıranlarının kıyı çizgisi üzerindeki modelle tahmin edilen etkileri uygulama ile karşılaştırmalı olarak tartışılmıştır.

Anahtar Kelimeler: Kıyı Çizgisi Değişimi, Kıyı Boyu Katı Madde Taşınımı, Açık Deniz Dalgakıranı, Tek-çizgi Teorisi

To My Family

To My Fiancée

ACKNOWLEDGEMENTS

I wish to express my gratitude to Prof.Dr. Ayşen Ergin, Assoc.Prof.Dr. Ahmet Cevdet Yalçıner and Dr. Işıkhan Güler for their very valuable supervision, support and recommendations throughout the study. I am grateful not only for their instructions and guidance in the courses from which I learnt the fundamentals of Coastal Engineering Profession, but also for the privilege to work with them in the sincere *Coastal Engineering Society.*

I would like to thank to Assoc. Prof.Dr. Mehmet Ali Kökpınar and Dr.Yakup Darama, from State Hydraulic Works (DSI), since they kindly provided field data.

I give special thanks to my dear friends, Mr. Cüneyt Baykal and Mr. Ilgar Şafak for every moment of very enjoyable and qualified co-operations, discussions hitting the target and table tennis tournaments between the intervals of coastal sedimentation sessions. The fellowship grown from here will never end.

I wish to express that it was a pleasure to be in Coastal & Harbour Laboratory with the research assistants and the staff and thank to them for their helps and good-humored personalities.

I direct my thanks to my fiancée, Öge Başoğlan for her unique motivation, helps and patience during the thesis work.

Any kinds of words are inadequate to express my thanks to my family for their irreplaceable and superlative support and motivation. I am grateful for everything I have acquired from them.

TABLE OF CONTENTS

LIST OF TABLES

LIST OF FIGURES

LIST OF SYMBOLS

α_0	deep water wave approach angle
α_b	angle of breaking with respect to x-axis
$\alpha_{b,A}$	breaking angle at point A resulting from the left hand side source point I within the sheltered zone
$\alpha_{b,A}'$	breaking angle at point A' resulting from the right hand side source point within the sheltered zone
$\alpha_{b,o}$	the integrated breaking wave angle behind an offshore breakwater within the sheltered zone
$(\alpha_{b,o})_t$	modified integrated breaking angle due to transmission
α_{bs}	angle of breaking wave with respect to shoreline
α_{io}	wave angle coming to the tip of the offshore breakwater
α_s	angle between the shoreline and x-axis
α'	wave approach angle at any depth.
α_L	deep water wave angles approaching from the right to the left
α_R	deep water wave angles approaching from the left to the right
β	a calibration coefficient for wave breaking by van Rijn (2001)
γ_b	breaker depth index
θ	angle in degrees between the shadow line of the structure and the related point at the line of breaking
θ_{IA}	angle between the vertical and between the straight line points I and A
ρ	fluid density
ρ_S	density of the sediment

ξ_0	surf similarity parameter
ξ	angle difference between the linear path and the circular path at point A
Δx	spatial increment
Δt	temporal increment
Ω_b	breaker height index
a	empirically determined coefficient for wave breaking by Weggel (1972)
b	empirically determined coefficient for wave breaking by Weggel (1972)
b_0	spacing between wave rays at deep water
b'	the spacing at any depth
d	depth at anywhere
d_b	breaking depth
g	the gravitational acceleration
m	beach slope
m_{ref}	reference beach slope
n	sediment porosity
q_y	cross shore sand transport rate
t	time elapsed for shoreline evolution
u_m	maximum value of orbital velocity in the surf zone
v_l	longshore current velocity
y	offshore distance
A_p	sediment dependent scale parameter
B	length of the offshore breakwater
C_0	the deep water wave celerity
C_{g0}	deep water group velocity
C_b	Breaking wave velocity

C_{gb}	Group velocity at breaking line
C_L	virtual centerline which passes through the midpoint of the offshore breakwater
D_{50}	median grain size diameter
$D_{50,ref}$	reference sediment grain size
D_B	berm height
D_C	depth of closure
D_{LT}	depth of longshore transport
D_{TOT}	total length of shoreline affected
E_b	wave energy at breaking line
G	gap distance between the offshore breakwaters
G_b	width of transition zone on the breaking line
G_B	width of the transition zone
Ho	deep water wave height
$H_{s,0}$	significant deep water wave height
$H_{s,0}'$	unrefracted equivalent deep water wave height
$H_{s,12}$	significant wave height that is exceeded 12 hr per year
H_b	breaking wave height
H_{bd}	modified breaking wave height due to coastal structures
H_d	the diffracted wave height
H_i	wave height in the long term wave statistics
H_{in}	incoming wave height to the edge of the structure or the obstruction
$H_{,rms}$	root mean square wave height
H'	wave height at any depth
I_l	immersed weight of sediment transport rate
K	empirical dimensionless calibration coefficient for longshore sediment transport rate
K_1	coefficient for longshore sediment transport rate by van Rijn (2000)

K_2	coefficient for longshore sediment transport rate by van Rijn (2000)
K_d	the diffraction coefficient
K_{d1}	diffraction coefficients computed from the left end of the offshore breakwater
K_{d2}	diffraction coefficients computed from the left end of the offshore breakwater
K_{dt}	diffraction coefficient according to the transmission coefficient, K_t
$K_{d,L}$	integrated diffraction coefficient of the breakwater at the left side of the gap
$K_{d,I}$	diffraction coefficient at the grids of the intersection region
$K_{d,R}$	integrated diffraction coefficient of the breakwater at the right side of the gap
K_{grain}	coefficient for sediment grain size correction
$K_{grain,min}$	minimum value of coefficient for sediment grain size correction
K_r	the refraction coefficient
$K_{r,b}$	refraction coefficient at breaking point
K_s	the shoaling coefficient
K_{slope}	coefficient of correction beach slope
K_{swell}	coefficient for wave period correction for swell waves
K_t	transmission coefficient of an offshore breakwater
L	wave length at any depth
L_0	is the deep water wave length
$L_{b,A}$	wavelength at breaking point A
L_I	the wavelength at source point I (Figure 5.15)
L_{off}	wavelength at the depth of offshore breakwater
N	number of spatial increments
P_i	occurrence probability of wave with height H_i.
P_l	longshore component of wave power
Q	longshore bulk sediment transport rate

Q_R	transport rates to the right resulting from the waves coming from the left
Q_L	transport rates to the left resulting from the waves coming from right
Q_{Gross}	gross longshore sediment transport rate
Q_{Net}	net longshore sediment transport rate
$Q_{t,mass}$	dry mass longshore sediment transport in kg/s
S	distance between the shoreline and the offshore breakwater
S_b	the distance from the shoreline to the breaking line
S_m	concentrating parameter characterizing the degree of directional spread
T	the significant wave period
T_{ref}	reference wave period
T_s	significant wave period
T_{swell}	period of swell waves
V	volume
$V_{eff,L}$	effective longshore velocity including tide effect
$V_{tide,L}$	longshore velocity in the mid surf zone due to tide
$V_{wave,L}$	longshore current velocity due to waves including wind effect
X_B	distance between the offshore breakwater and salient apex
X_S	distance between the shoreline and the salient apex

CHAPTER 1

INTRODUCTION

To see a world in a grain of sand
And a heaven in a wild flower
Hold infinity in the palm of your hand
And eternity in an hour
William Blake

The fabulous intersection of the land and the sea, coastal zones have always been appealing to mankind for recreation, residence and transportation purposes. A high majority of the world population lives in very crowded metropolises which are established near or along the shore for both the ease of shipping and the natural instinct of mankind to live near the coasts. A significant portion of the population prefers living in small coastal towns or villages for vacation.

Nevertheless, spectacular coastal areas are facing a serious and ever-growing problem, namely erosion. Beach berms disappear, shoreline is recessed and the property losses happen resulting from severe erosion. Therefore, coastal defence and the measures to be taken in order to prevent erosion and to provide sheltered areas have interested many researchers, and as a result, various studies and literature have emerged on these raised issues for a few decades.

Coastal defense and stabilization works are designed to retain or rebuild natural systems (cliffs, dunes, wetlands, beaches) or to protect man's property (buildings, infrastructure, etc.) landward of the shoreline (CEM, 2003).

Despite the fact that there are many important aspects to coastal zone management, such as the environment, transportation, economics, biology, etc. the most significant and the ultimate design criterion is often the movement of sediment (Kamphuis, 2000).

Many scientists have worked on coastal sedimentation to foresee the behavior of shoreline, which is influenced by integration of wave, current, sediment, beach and coastal structure (if any) parameters. The choice of the policy to protect the beach against erosion is a difficult criterion to decide. Hard measures, i.e. coastal structures such as groins, jetties, seawalls, offshore breakwaters, and submerged breakwaters can be constructed, as well as soft measures like artificial beach nourishment may be applied. Great care should be paid before designing structures since they do contribute no amenity, but harm to the adjacent beach. In some cases combination of a structure and beach fill, for example a series of groin accompanied by a beach fill, may serve the best protection for the site of concern.

Before designing a coastal project, firstly a thorough understanding of the project site, wave climate, currents, sediment and beach characteristics, sediment budget and the features of the structures which are proposed to be constructed, should be comprehended entirely by the designer.

Structure should only be built once the physical system is well understood; otherwise the structure is just a “full-scale experiment”. It should be always kept in mind that the system is permanently altered by any hard structures and the sand formations in their lee (Black, 2003).

It is quasi impossible to fully predict the exact future beach planform of a site under the combined effects of wave climate and structure combinations, owing to the complexity of the problem, the uncertainties of the data, and the specific conditions of the particular site. However there might be a chance to orient all the parameters in a logical manner to predict the future shoreline with basic assumptions. This is possible using physical or numerical engineering tools. Comprehensive results are obtained quantitatively and qualitatively by various researchers through field and laboratory measurements as well as numerical experiments.

In order to interact the wave, sediment and structural variables to see their effects in time dependent trend of shoreline change, numerical models of shoreline evolution have been commonly used (Hanson and Kraus, 1991). Numerical models, being both low-cost and less time consuming, are easy to use tools in an office environment which provides the researcher with visualizing the long term shoreline evolution in the scope of the assumptions and limitations of one-line theory and enhancing the engineering intuition about the inside story of the nearshore processes and longshore sediment transport phenomenon. Additionally they are free from scaling problems of the physical models in laboratory experiments, indicated by Hanson (1987).

A numerical model should catch the behavior of beach planform for the structures and exposed wave climate qualitatively well matching with the field data. Calibration and improvement of the numerical model may be performed after attaining adequate number of qualitative agreements with field measurements for generalizing the model for a variety of combinations of irregular shorelines and structure systems to reach quantitatively comparable predictions with the actual change in the shoreline.

In this respect, it is aimed to achieve consistent and beneficial long term predictions of shoreline evolution under the wave, sediment, current, structure interaction by a numerical model developed herein, which is based on one-line theory in this study.

One-line theory principles will be introduced in Chapter 2 together with the background, literature review and the basic assumptions and limitations. Fundamental relationships, the finite difference scheme to approximate the differential equations are going to be discussed.

In Chapter 3 the transformation of waves from deep water to the surf zone where they break is going to be held. Wave shoaling, wave refraction and diffraction are briefly discussed at the beginning; then, breaking phenomenon is going to be focused on since it is the governing design parameter in the majority of coastal

stabilization projects. Researchers and their breaking criteria will be held from the point of view of their applicabilities to generalized cases in the numerical model.

In Chapter 4, longshore sediment transport will be introduced conceptually and bulk sediment transport expressions will be discussed with respect to their derivations and capability to cover the related basic parameters. Then comparison will be made among the expressions, which are developed by SPM (1984), Kamphuis (1991) and van Rijn (2002).

In Chapter 5, the capability of the model with the coastal structures is going to be indicated. Introduction of offshore breakwaters into the numerical model is explained in detail and T-shaped groins are briefly discussed. A review of empirical studies of researchers based on both the field and the laboratory results are presented. In the development of the numerical model, the diffraction patterns affecting breaking wave heights and the breaking angles behind a single offshore breakwater and multiple offshore breakwater systems will be presented in detail. Introduction of wave transmission through offshore breakwaters is going to be presented. Sample runs are going to be carried out and presented for single and multiple offshore breakwater systems.

In Chapter 6, a comparative study is carried out for proposing hypothetical offshore breakwaters for an application with groins in which the numerical model results are qualitatively in good agreement with the measured field data.

In the Chapter 7, the conclusion and discussion of the results will be presented together with the recommendations for future studies.

CHAPTER 2

ONE-LINE THEORY

2.1 General Overview and Background

The seasonal variations in wave climate cause sediment to be transported cross-shore leading to changes in bottom profile. However, unless a very destructive storm happens, the change in the profile returns to its pre-storm shape in a short time such that the shape of the profile remains constant over a long period (Hanson, 1987).

Within the light of the basic assumption of an unchanged beach profile considered in long term scale, the beach profile, keeping stable, moves parallel to itself either onshore (causing erosion) or offshore (leading accretion), up to a depth, so-called depth of closure, the offshore side of which is free from sediment motion or has so little sand movement that can be neglected.

All the contours extend parallel to the shoreline and move the same distance, since the profile is constant in shape. Therefore one-line modeling uses a single line as the name implies and practically the shoreline is taken as the one dimensional contour line to represent the complete beach movement (Kamphuis, 2000).

Pelnard-Considere (1956) was the first to introduce one-line theory. There are many researchers who have studied on one-line theory after that time and the recent numerical models based on one-line theory are given in Kamphuis (2000) which are the ones developed by Perlin and Dean (1983), GENESIS by Hanson

and Kraus (1989) and ONELINE by Kamphuis (1993), Dabees and Kamphuis (1998), and Dabees (2000).

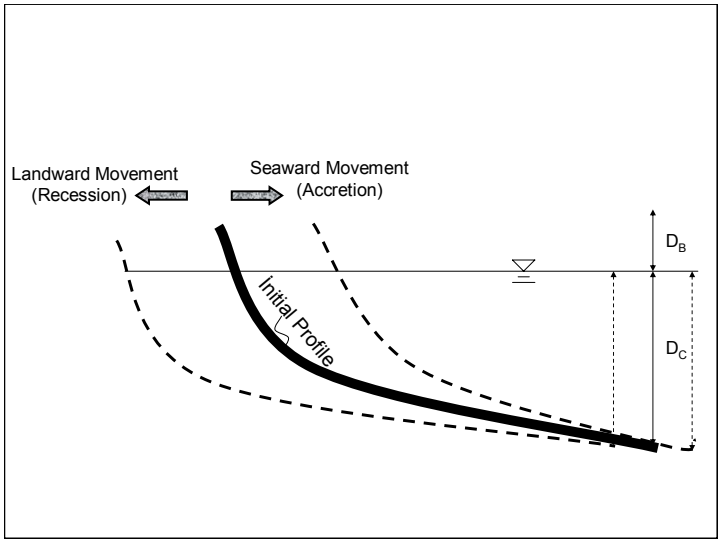

Figure 2.1 *Bottom profile and change of shoreline*

In *Figure 2.1*, it is seen that the profile is constant down to the depth of closure and the initial profile, as a block, moves seaward or landward, where D_B is the berm height and D_C is the depth of closure.

If the longshore variations of shoreline dominate the short term fluctuations of shape of beach profile, one-line modeling is very well applicable and gives reasonable results in the vicinity of coastal structures (Hanson, 1987).

2.2 Assumptions and Limitations

The basic assumption of one-line theory is the unchanged profile in long term scale up to a depth of closure, which focuses on the longshore sediment transport

for shoreline evolution as explained above. However this assumption loses its validity when a strong storm changes the profile and the profile does not return to its pre-storm shape in a long time.

One-line theory accounts for the longshore sediment transport rate, and it is assumed that the longshore sediment transport is engendered by only oblique breaking waves and wave driven longshore currents (Hanson, 1987).

Moreover, to attain reasonable estimates of predicted shorelines with the numerical models, small breaking angles should be used in the numerical model based on one-line theory. Also using small angle of shoreline change is important in modeling to get stable results (Dabees, 2000).

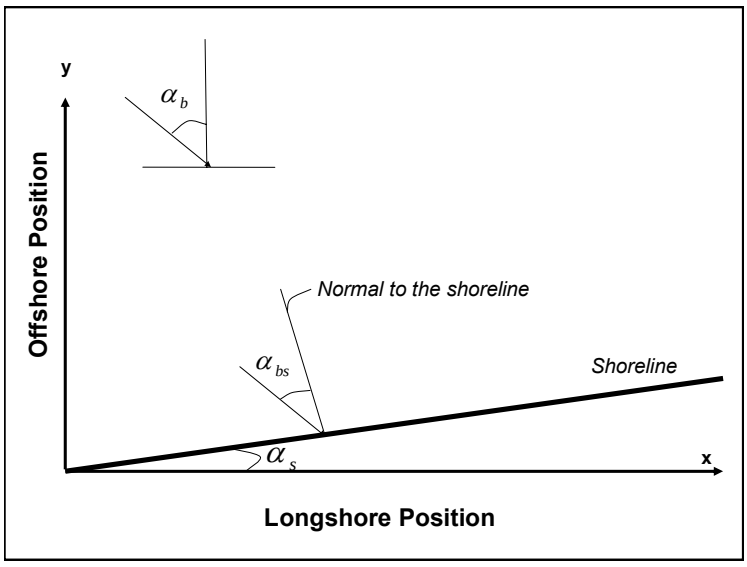

Figure 2.2 *Breaking angles with respect to shoreline*

$$\alpha_{bs} = \alpha_b - \alpha_s \qquad (2.1)$$

where α_b is the angle of breaking with respect to x-axis, α_s is the angle that shoreline makes with x-axis and α_{bs} is the angle of breaking with respect to shoreline as seen in *Figure 2.2.*

Offshore losses and/or gains to the sediment budget are neglected within the numerical model developed. Also it is assumed that no reflection takes place in front of the structures. Besides, the longshore sediment transport rates at the two edge grids of the beginning and the end of the shorelines are assumed to be equal to each other which implies no shoreline change with time ($\partial y / \partial t = 0$) implying ($\partial Q / \partial x = 0$) as a result of *Eqn.(2.4)* such that $Q_1 = Q_2$ and $Q_{N+1} = Q_N$ where y is the shoreline position onshore or offshore Q is the longshore sediment transport rate and the subscripts denote spatial grids and N is number of spatial increments in the longshore direction.

2.3. Basic Relationships of One-line Theory

Sand continuity equation is used to account for the shoreline change, i.e. alongshore movement which is described below.

$$\delta V = \left\{ Q - \left(Q + \frac{\partial Q}{\partial x} \partial x \right) + q_y \right\} \partial t \qquad (2.2)$$

where V is the volume, y is the offshore shoreline position (+) if towards seaward , x is the alongshore coordinate, t is the time for shoreline evolution, Q is the longshore bulk sediment transport rate, q_y is onshore-offshore sand transport rate (+if onshore), which accounts for river or creek discharges as well as sinks and net cross-shore losses if any.

$$\partial V = \partial y \cdot (D_C + D_B) \cdot \partial x \qquad (2.3)$$

can be written from the geometry where D_C is the depth of closure and D_B is the berm height. Solving these two equations simultaneously above, governing equation for the one-line model of shoreline changes is obtained.

$$\frac{\partial y}{\partial t} = -\frac{1}{D_c + D_B}\left(\frac{\partial Q}{\partial x} + q_y\right) \qquad (2.4)$$

If onshore-offshore transport rate is q_y *=0* for long-term changes, *Eqn. (2.4)* is reduced to

$$\frac{\partial y}{\partial t} + \frac{1}{D_C + D_B} \cdot \frac{\partial Q}{\partial x} = 0 \qquad (2.5)$$

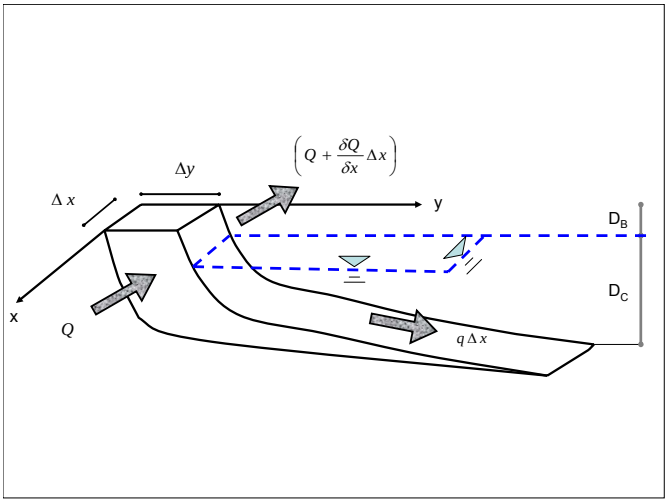

Figure 2.3 *Definition sketch of conservation of mass*

The governing differential *Eqn. (2.5)* will be approximated by explicit scheme finite difference methodology. The time derivative of y is approximated by forward difference methodology. $\partial y / \partial t$ is approximated by $\left(y_i^{j+1} - y_i^j\right)/\Delta t$ and similarly, the term $\partial Q / \partial x$ is approximated by $\left(Q_{i+1}^j - Q_i^j\right)/\Delta x$ in which forward

difference methodology for spatial variable is used. And rewriting the governing differential equation with the approximated derivatives, we obtain

$$\frac{y_i^{j+1} - y_i^j}{\Delta t} + \frac{1}{D_C + D_B} \cdot \frac{Q_{i+1}^j - Q_i^j}{\Delta x} = 0 \qquad (2.6)$$

Arranging it for the next time step of the shoreline position, *Eqn. (2.7)* is attained.

$$y_i^{j+1} = y_i^j - \left(\frac{1}{D_C + D_B} \right) \cdot \left(Q_{i+1}^j - Q_i^j \right) \cdot \frac{\Delta t}{\Delta x} \qquad (2.7)$$

where Δx is the spatial increment and Δt is the temporal increment.

In *Eqn. (2.7)*, the wave climate and beach parameters are kept constant to compute the change of shoreline hence the longshore sediment transport rate in the present time step *(j)*. Then this change is added to the initial shoreline in the present time step *(j)* to reach the new shoreline in the next time step *(j+1)*. The subscript *(i+1)* denotes for the next grid in the spatial dimension.

In the explicit scheme solution, great care should be paid for model stability. The grid spacing and time step required are determined according to this stability condition. In Dabees (2000), it is stated that the stability is critically limited to small time steps in explicit scheme and the stability condition is given as follows.

$$\frac{Q}{\alpha_b (D_C + D_B)} \frac{\Delta t}{\Delta x^2} \leq \frac{1}{2} \qquad (2.8)$$

Although the continuity equation does not need the shape of the bottom profile, it is required to calculate the average bottom slope (Hanson, 1987). Dean (1977)

proposed a bottom profile equation also denoted as “Dean profile” which is given in *Eqn. (2.9)*

$$d = A_P \cdot y^{\frac{2}{3}} \qquad (2.9)$$

where y means the offshore distance from the shoreline and d is the depth at that offshore distance *(y)*, and A_p is a scaling parameter *($m^{1/3}$)* which is a function of median grain size diameter *(D_{50}).*

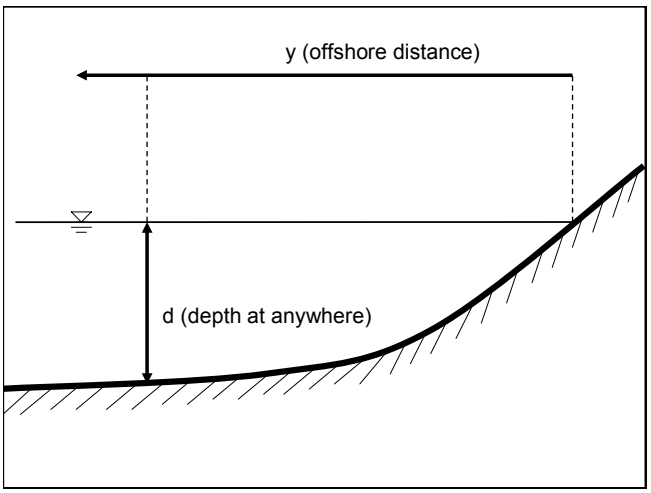

Figure 2.4 *Definition sketch for* ***“****Dean profile”*

In Kamphuis (2000), A_p and the beach slope (*m)* is given as follows

$$A_p = \left(1.04 + 0.086 \cdot \ln\left(D50\right)\right)^2 \quad \text{for } 0.1\text{x}10^{-3}\text{m.} \leq \text{D}_{50} \leq 1\text{x}10^{-3}\text{ m.} \qquad (2.10)$$

$$m = \frac{2}{3} A_p^{\frac{3}{2}} d_b^{-\frac{1}{2}} \qquad (2.11)$$

where d_b is the breaker depth. Beach slope of the surf zone is defined from the shore to the immediately offshore of the breaking line in *Eqn. (2.11),* which is taken as the tangent line of the profile at that point (Kamphuis, 2000).

The depth of closure, beyond which the sediment motion is supposed to be negligible, is formulated by Hallermeier (1978) as follows:

$$D_c = 2{,}28H_{s,12} - \frac{68{,}5\left(H_{s,12}\right)^2}{gT^2} \qquad (2.12)$$

where $H_{s,12}$ is the non-breaking significant wave height that is exceeded 12 hr per year (0.137% of the time), T is the significant wave period, and g is the gravitational acceleration.

Hanson (1987) defined a "depth of longshore transport", (D_{LT}) which is associated with a short term basis (hours). Depth of longshore transport accounts for only longshore sediment transport and beyond this depth no sediment will move due to only longshore transport. In the numerical model GENESIS, Hanson (1987) utilized the Hallermeier's formula *Eqn. (2.12)* with deep water wave height $H_{s,0}$ instead of $H_{s,12}$ for depth of longshore transport (D_{LT}), since D_C should be evaluated over a longer period and it is the depth beyond which sediment motion caused by any process (longshore transport, cross-shore transport etc.) is ignorable. In the numerical model herein, Hanson's approach of "depth of longshore transport" is used such that breaking wave height (H_b) is used instead of $H_{s,12}$ in *Eqn. (2.12).*

$$D_{LT} = 2{,}28H_b - \frac{68{,}5\left(H_b\right)^2}{gT^2} \qquad (2.13)$$

CHAPTER 3

WAVE TRANSFORMATION AND BREAKING

3.1 Shoaling

As the waves propagate shoreward, the water depth gets shallower and the wave heights and the wave lengths are affected by this effect, which is called shoaling. Shoaling effect can be reflected by the coefficient of shoaling which relates the wave height at any depth to deepwater wave height.

$$K_s = \frac{H'}{H_{s,0}} \qquad (3.1)$$

where H' and $H_{s,0}$ are the wave heights at any depth and deep water, respectively and K_s is the shoaling coefficient.

3.2 Refraction

Oblique waves are subject to refraction process in addition to shoaling. Under the assumption of straight and parallel bottom contours, the wave crest propagates obliquely to the shore and the ends of the wave crest are at different depths. The farther end with respect to the shoreline is at a deeper location and hence has a greater velocity than the closer side of the crest with respect to the shoreline. This situation leads to bending of wave crest, which is called refraction (Kamphuis, 2000). The refraction coefficient is derived from the simple geometric relationships to compute the wave height at the related depth from the deep water wave height.

$$K_r = \sqrt{\frac{\cos\alpha_0}{\cos\alpha'}} \qquad (3.2) \qquad K_r = \sqrt{\frac{b_0}{b'}} \qquad (3.3)$$

where b_0 is the spacing between wave rays at deep water, b' is the spacing at any depth. In the same manner α_0 is the deep water wave approach angle and α' is the wave approach angle at any depth.

3.3 Diffraction

Waves reduce their energy to some extent and the wave heights and wave directions are altered correspondingly when they come across a natural obstacle or a coastal structure on their route to the shoreline. This situation is called the wave diffraction. The extension of wave ray reaching the edge of the structure separates the outer zone and the shadow zone. The lateral energy is transferred into the shadow region of the structure, which is the protected zone by the structure. To compute the reduction in wave height, diffraction coefficient, K_d is used such that

$$K_d = \frac{H_d}{H_{in}} \qquad (3.4)$$

where H_d is the diffracted wave height and H_{in} is the incoming wave height to the edge of the structure or the obstruction.

3.4 Breaking

3.4.1 Wave Breaking Concept

The lifetime of an individual wave shows similarity with that of a man in the milestone events along its route to the shoreline. Waves are generated by wind along fetch lengths, like birth of a human, and they propagate towards the shoreline keeping their forms unchanged until they reach the deep water limit

according to linear wave theory. After this limit, they start to change in height, length and direction with the suite of the transformation phenomena which are shoaling, refraction and diffraction. Finally the most hydrodynamic mechanism in the surf zone, breaking takes place which can be regarded as the end of the lifetime of that individual wave. As seen, an individual wave is born, grows up, changes shape, decays after breaking and reaches the shoreline, which resembles all the milestones of a lifetime like a member of a mankind experiences.

Wave breaking phenomena is the most important wave transformation concept in coastal stabilization, since breaking waves are considered to be the most energetic and destructive waves and used to be the governing design parameter for the structural stability of coastal defence structures. Breaking waves are also regarded as the dominant parameter used in computation of longshore sediment transport rate and thus predicting the shoreline since they generate a pronounced momentum and stir the sediment below (Kamphuis, 2000). Wave transformation from deep water to the breaker depth is a complex process. Several literatures have emerged on this topic over a century. Wave breaking height *(H_b)* is a function of water depth *(d_b)*, wave steepness *(H/L)*, beach slope *(m)* and the approaching deep water wave angle (α_0).

Waves increase in steepness as they come closer to the shore, i.e. as the water depth decreases. Wave steepness can increase up to a physical limit for which the wave may keep its stability. When the maximum steepness is exceeded, waves break dissipating their energy and leading to nearshore currents and increased mean water level in the surf zone (CEM, 2003). The depth where the waves break is called the breaker depth (*d_b)*, which is in the same order of magnitude with breaking wave height (*H_b)*. The threshold steepness, after which the waves break, is proposed by Miche (1944) for horizontal sea bottom in *Eqn. (3.5)*

$$\left(\frac{H}{L}\right)_{\max} = \frac{1}{7}\tanh\left(2\pi\frac{d}{L}\right) \qquad (3.5)$$

where *H/L* is the steepness, *d* is the water depth and *L* is the wave length at any point of wave propagation from deep water to the shore.

The surf zone is described as the region from the limit of wave uprush to the seaward end of the breaking point as shown in *Figure 3.1*. The sediment movement and hence the bathymetry change are in their peak rates by the effect of breaking waves and the nearshore currents in the surf zone. Therefore, in order to predict shoreline evolution, to design coastal structures and beach fills, and to estimate storm damages, breaking wave height (H_b), the breaker depth (d_b) and the angle of breaking (α_b) are of first importance to be calculated. Nearshore currents, which occurred due to wave breaking should be evaluated for better predictions and designs (CEM, 2003).

There are various definitions for wave breaking. The famous definition is the point where the wave height is in its maximum value. Munk (1949) expresses that waves break when the particle velocity at the wave crests is greater than the wave celerity. The waves are also known to break where the white capping or foam occurs, or where the front slope of the breaking is almost vertical.

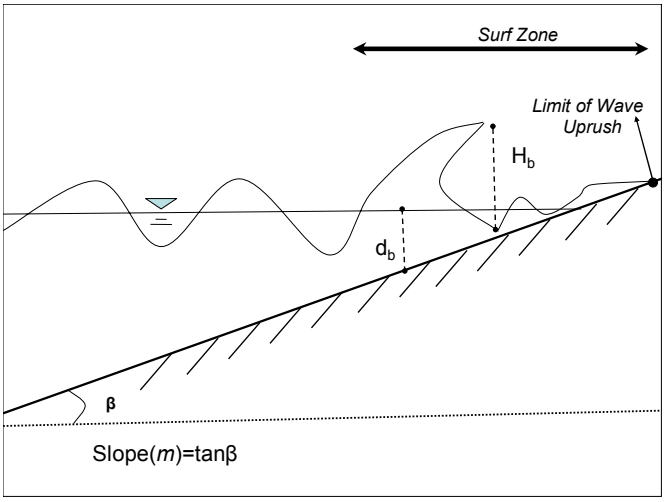

Figure 3.1 *Definition sketch for breaking wave height and depth*

There are two criteria for breaking index, which are used to non-dimensionalise the breaking wave height. The breaker depth index (γ_b) is the ratio of breaking wave height to the breaker depth as shown in *Eqn. (3.7)* (CEM, 2003).

$$\gamma_b = \frac{H_b}{d_b} \qquad (3.6)$$

The breaker depth index (γ_b) is proposed theoretically by Mc Cowan (1891) and Munk (1949) to the upper limit value of 0.78 by solitary wave theory for horizontal bottom

$$\gamma_b = 0.78 \qquad (3.7)$$

This value has a wide range practical usage in engineering applications as a first estimate (CEM, 2003). Collins (1970) has developed an expression for breaker depth index including the beach slope based on his observations. The expression is as follows.

$$\gamma_b = 0.72 + 5.6\, m \qquad (3.8)$$

The other non-dimensional breaker criterion is the breaker height index (Ω_b) which is the ratio of the breaking wave height (H_b) to the deep water wave height ($H_{s,0}$) as expressed in *Eqn. (3.9)* (CEM, 2003).

$$\Omega_b = \frac{H_b}{H_{s,0}} \qquad (3.9)$$

Breaker type is the shape of the wave crest during breaking. Breaking waves are divided into four categories according to their forms of breaking as spilling, plunging, collapsing and surging breakers (Galvin, 1968). The first type of breakers is the spilling breakers, in which wave crests are slightly lowered and white-capping occurs in the wave crest. Spilling breakers occur when the wave

steepness is high and the bottom slope is quite flat. In plunging breakers the wave crest moves forward compared to its base in a curled way as shown in *Figure 3.2*. Plunging waves occur on steeper beaches exposed to waves having intermediate steepness. The third type of breaking is the collapsing breakers in which wave crests keep stable and unbroken and the lower part of the shoreward face becomes steep for a while and then suddenly falls down. Collapsing breakers occur on a reasonable steep slope with low steepness waves. The last type of breakers, surging breakers appear on very steep beaches. The waves only goes up and come down along the slope with a very little or no breaking. Extreme low steepness waves break in surging type or they even may not break and turn into standing waves by reflecting back from the beach (CEM, 2003).

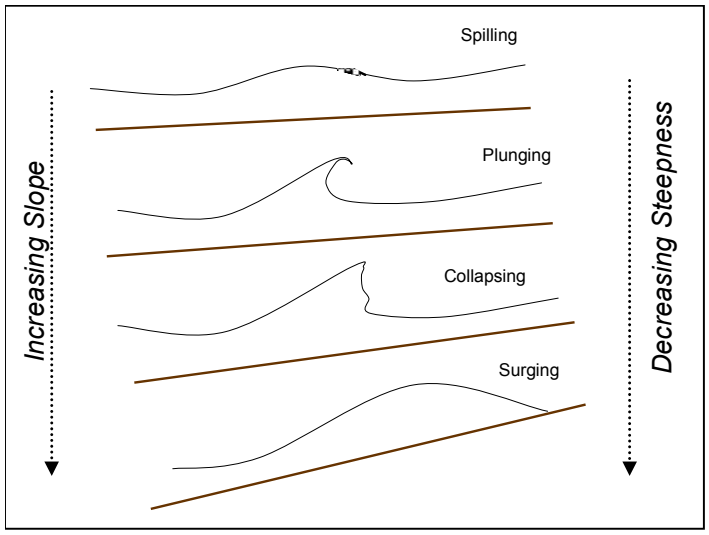

Figure 3.2 *Types of breakers*

In order to distinguish between breaker types, Irribarren number or so-called surf similarity parameter is used. Irribarren number is a function of beach slope and wave steepness as seen in *Eqn. (3.10)*.

$$\xi_0 = \frac{m}{\sqrt{\frac{H_{s,0}}{L_0}}} \qquad (3.10)$$

where L_0 is the deep water wave length calculated from $L_0 = (g / 2\pi) \cdot T^2$, m is the beach slope. Through the expressions of *Eqn. (3.11)* from bottom to top with increasing slope and decreasing wave steepness, the following distinction can be made between the types of the breakers (Ergin, 1998).

For $\xi_0 < 0.5$	spilling breakers	*(3.11.a)*
For $0.5 < \xi_0 < 2.5$	plunging breakers	*(3.11.b)*
For $2.5 < \xi_0 < 3.4$	collapsing breakers	*(3.11.c)*
For $3.4 < \xi_0$	surging breakers	*(3.11.d)*

Bodge and Dean (1987) state that longshore sediment transport should be related to the breaker type in any wise. Wang et al., (2002) found large difference in longshore sediment transport rates at breaker line between the plunging and spilling breakers in the laboratory work and they attributed this difference to much higher sediment concentrations in the water column that were created by the plunging breakers. Moreover their experiments indicated that in the swash zone, differences seem to be attributed to the much higher energy of the uprush and downrush associated with the longer-period waves which are more likely to be the plunging type breakers.

3.4.2. Wave Breaking Theories and Relationships

Wave breaking has attracted many researchers since the dominancy of the process for coastal defence is remarkable. Here, it is aimed to review the literature on wave breaking phenomenon and decide on the breaking expression to be used in the numerical model. Different approaches and the theories behind them will be discussed for wave transformation along the surf zone. Then the computed results using each relationship for breaking parameters (H_b, d_b, and α_b) are going to be compared, for a suite of wave and beach inputs, with changing only one input parameter and keeping the rest constant.

3.4.2.1 Munk (1949)

Munk (1949) has derived the expression for the breaker height index of a solitary wave.

$$\frac{H_b}{H_{s,0}} = 0.30 \times (\frac{H_{s,0}}{L_0})^{-1/3} \qquad \textbf{(}3.12\textit{)}$$

By means of *Eqn. (3.12)*, anyone may reach a practical value of breaking wave height *(H_b)* for a given period and a deep water significant wave height *($H_{s,0}$)*. Breaker depth index , γ_b=0.78 is used.

3.4.2.2 Komar and Gaughan (1973)

Komar and Gaughan (1973) have derived a semi-empirical relationship for the breaker height index using linear wave theory.

$$\frac{H_b}{H_{s,0}} = 0.56 \times (\frac{H'_{s,0}}{L_0})^{-1/5} \qquad (3.13)$$

where $H_{s,0}$' is the unrefracted equivalent deep water wave height and it is given by *Eqn. (3.15)*

$$H_{s,0}' = K_{r,b} \cdot H_{s,0} \qquad (3.14)$$

where $K_{r,b}$ is the refraction coefficient at breaking point. Assuming the initial value of refraction coefficient at the breaking line such that $K_{r,b}$ equals to 1 and assuming the initial breaking angle equal to the deep water approaching angle *Eqn. (313)* can be solved iteratively, and to compute the breaker depth, γ_b=0.78 is used here also.

3.4.2.3 Weggel (1972)

The assumption of horizontal bottom rarely reflects the real situations. Thus the effect of the beach slope *(m)* for computation of breaking wave parameters is included in the later studies. For example Weggel (1972) has developed an empirical expression from laboratory data on monochromatic waves breaking on smooth, plane slopes, for $m \leq 0.1$ and for $H'_{s,0}/L_0 \leq 0.06$.

$$\gamma_b = \frac{H_b}{d_b} = b - a \cdot \frac{H_b}{gT^2} \qquad (3.15)$$

$$a = 43.8 \cdot (1 - e^{-19m}) \qquad (3.16)$$

$$b = \frac{1.56}{(1 + e^{-19.5m})} \qquad (3.17)$$

The parameters *a* and *b* are empirically determined coefficients as functions of beach slope *(m). Eqn. (3.15)* may be used to compute breaker index by using the wave height calculated from *Eqn.(3.13)* and then compute the breaker depth index and compute the breaker depth.

3.4.2.4 Kamphuis (2000)

Kamphuis (2000) proposed two criteria for wave steepness and depth limited criteria, which are extended versions of *Equations (3.5)* and *(3.6)* respectively. The expressions were obtained for irregular waves, based on model testing. Kamphuis has also included the beach slope *(m)* to the wave transformation in the surf zone. The expressions for wave steepness (H_b/L_b) and depth limited (H_b/d_b) criteria are as follows:

$$\frac{H_b}{L_b} = 0.095 \times e^{4.0m} \times \tanh\left(\frac{2\pi d_b}{L_b}\right) \qquad (3.18)$$

$$\frac{H_b}{d_b} = 0.56 \times e^{3.5m} \qquad (3.19)$$

where L_b is the breaking wave length

3.4.2.5 Goda (1985)

For regular waves, the location of wave breaking, i.e. the breaking point, the breaker depth and the breaking height is almost fixed. But in contrast with regular waves, random (irregular) waves break in a wide spatial range. Goda (1985) states that the wave transformation in the surf zone is a difficult to express owing to the wakes, turbulence and air entrainment processes. Goda has used the Rayleighan probability distribution for wave heights before breaking. The waves entering the surf zone will not conform to the distribution due to breaking. Therefore redistribution of wave heights is required by removing the portion of waves breaking from the original distribution. In this process, irregular wave rays are supposed to break showing a fluctuation in wave height due to variation of individual periods and other characteristics. Within the light of this approach, Goda obtained a relationship for wave breaking including beach slope in *Eqn. (3.20)*, after compilation of laboratory results.

$$\frac{H_b}{L_0} = A \cdot \left[1 - e^{-\left\{ \frac{1.5\pi d_b}{L_0}\left(1 + 15\ m^{4/3}\right)\right\}} \right] \qquad (3.20)$$

In *Eqn. (3.20)*, A is a coefficient changing from 0.18 (the upper limit of breaking) to 0.12 (the lower limit of breaking) in consideration of the variability of irregular waves. But it is taken 0.17 as Goda suggests for regular waves. *Eqn.(3.20)*, is solved iteratively such that, the initial value of breaker depth (d_b) can be assigned to significant deep water wave height since they are in the same order of magnitude and then breaking wave height is calculated. The second value of breaker depth can be calculated by the breaker depth index proposed by *Eqn.*

(3.7). Iteration should go on until negligible difference is achieved between the two successive calculated breaker depths.

3.4.2.6 Le Mehaute and Koh (1967)

Le Mehaute and Koh (1967) have developed a breaking wave criterion taking into account the effects of the beach slope based on experimental data.

$$\frac{H_b}{H'_{s,0}} = 0.76 \times (m \times \cos(\alpha_b))^{1/7} \times (\frac{H'_{s,0}}{L_0})^{-1/4} \qquad (3.21)$$

As it is the case in *Eqn. (3.13),* assuming the initial value of refraction coefficient at the breaking line, $K_{r,b}$ equals to 1 and assuming the initial breaking angle equal to the deep water approaching angle, *Eqn. (3.21)* can be solved iteratively for breaking parameters. In *Eqn. (3.21)*, experimental data points used are limited to the slope and wave steepness for the ranges of $0.02 < m < 0.2$ and $0.002 < H_{s,0}/L_0 < 0.09$.

3.4.2.7 CEM (2003)

Wave transformation in the surf zone, assuming that the offshore bottom contours are straight and parallel to the shoreline is presented in CEM (2003). Also the energy loss before breaking is neglected. Conservation of wave energy principle is used to obtain breaking wave height, given in *Eqn. (3.22)* and Snell's law is used to obtain breaking wave angle in *Eqn. (3.23).*

$$H_b = H_{s,0} \cdot \left[\frac{C_{g0} \cdot \cos\alpha_0}{\sqrt{\frac{g}{\gamma_b} \cdot \cos\alpha_b}} \right]^{2/5} \qquad (3.22)$$

$$\sin\alpha_b = C_b \cdot \frac{\sin\alpha_0}{C_0} \qquad (3.23)$$

where C_0 is the deep water wave celerity given in *Eqn. (3.24)*, deep water group velocity, C_{g0} is given by *Eqn. (3.25).* Shallow water wave velocity (C_b) is approximated as in small amplitude linear wave theory in *Eqn. (3.25). Group* velocity at breaking line (C_{gb}) is also has the same value with (C_b) assuming breaking depth is a shallow water depth.

$$C_0 = \frac{L_0}{T} \qquad (3.24) \qquad\qquad C_{g0} = 0.5 \cdot \frac{L_0}{T} \qquad (3.25)$$

$$C_b = C_{gb}\sqrt{gd_b} \qquad (3.26)$$

Equations *(3.22)* and *(3.23)* can be combined to form

$$H_b = (H_{s,0})^{4/5} \times (C_{g0} \cdot \cos(\alpha_0))^{2/5} \left[\frac{g}{\gamma_b} - \frac{H_b \cdot g^2 \cdot \sin^2(\alpha_0)}{\gamma_b^2 \cdot C_0^2} \right]^{-1/5} \qquad (3.27)$$

where γ_b is the breaker depth index and it is used with the well-known practical value of 0.78 given in *Eqn. (3.7)*. Formula of CEM (2003), *Eqn. (3.27)* can be solved iteratively for H_b and then breaking wave angle can be found using *Eqn. (3.23).*

3.4.2.8 Van Rijn (2002)

Van Rijn (2002) follows a methodology in which breaking line is assumed to be the location where 5% of the waves are breaking.

$$d_b = \left(\frac{{H_{s,0}}^2 \cdot C_0 \cdot \cos\alpha_0}{\beta \cdot {\gamma_b}^2 \cdot g^{0.5}} \right)^{0.4} \qquad (3.28)$$

where β=1.8 a calibration coefficient based on field data. A different breaker depth index value is used by van Rijn as $\gamma_b = H_b / d_b$ =0.4 since it is based on breaking line assumption mentioned above.

3.5 Comparison of Breaking Theories

It is obvious that wave steepness (H_0/L_0), deep water approach angle (α_0), and beach slope (*m)* dictate the breaking depth and thus breaking wave height and angle. In order to decide among the theories of Munk, Komar & Gaughan, Weggel, Kamphuis, Goda, Le Mehaute & Koh, CEM, and van Rijn, to be used in the numerical model, some computations are carried out to compare the results of breaking wave characteristics. Firstly using these different breaking theories curves are plotted as it is seen in *Figure 3.3* in which the ratio of breaking wave height to deep water wave height for different steepness values is presented for deep water approach angle, α_0=0˚ and beach slope, *m*=1/30.

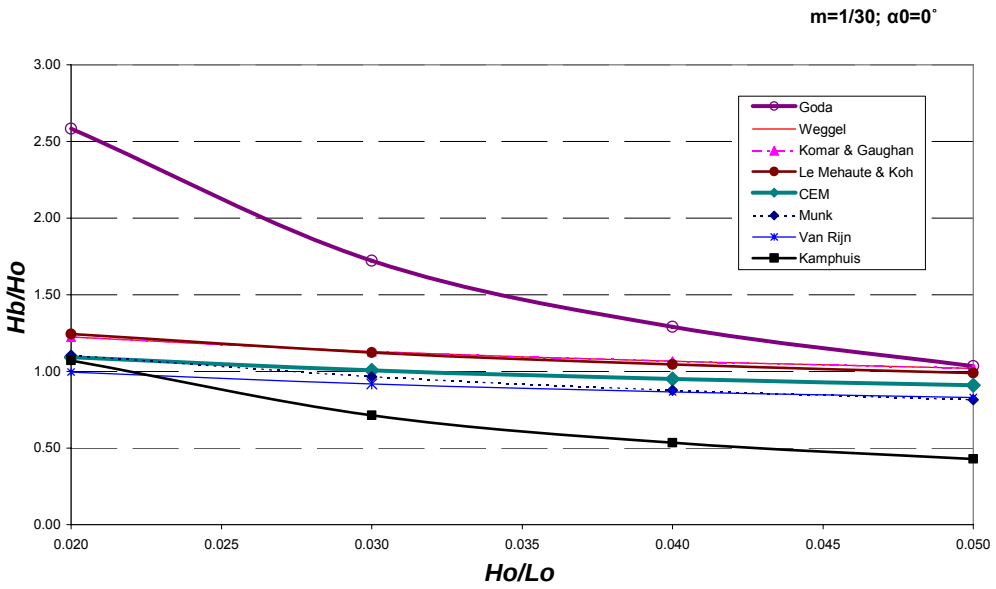

Figure 3.3 H_b/H_o vs. Steepness for α_0=0˚ & m=1/30.

As it is seen from *Figure 3.3* curves plotted using Goda's and Kamphuis's methodology are enveloping curves where Goda gives the maximum results. The recently given CEM (2003) breaking theory results are in agreement with Munk, Komar &Gaughan, Weggel, Le Mehaute & Koh and van Rijn all of which are within the enveloping curves.

Moreover, breaking wave parameters such as breaking wave height *(H_b)*, breaking depth *(d_b)*, breaker depth index (γ_b) and breaking wave angles (α_b) are computed for a set of wave parameters ($H_0/L_o, \alpha_0$, m) for different breaking theories. In the first three data set through *Tables 3.1.A to 3.1.C*, wave steepness and beach slope *(m)* are kept constant, only the deep water approach angle (α_0) is changed, whereas in the last 3 data sets through *Tables 3.1.C to 3.1.E*, wave steepness and deep water approach angle are kept constant and the beach slope is changed.

Table 3.1.A *Results obtained from Input Set #1*

INPUT SET #1				**H_0 *(m)***	**T (s)**	**α_0**	**H_0/L_0**	**m**
				1.5	**4.78**	**60˚**	**0.042**	**1/50**
	Munk	Komar & Gaughan	Weggel	Kamphuis	Goda	Le Mehaute & Koh	CEM	Van Rijn
H_b (m)	1.29	1.67	1.67	0.68	1.17	1.13	1.12	0.98
d_b (m)	1.66	2.14	2.02	1.13	1.50	1.36	1.43	2.44
γb	0.78	0.78	0.83	0.60	0.78	0.83	0.78	0.40
α_b	26.40˚	29.90˚	29.05˚	21.91˚	25.11˚	23.98˚	24.60˚	31.77˚

Table 3.1.B *Results obtained from Input Set #2*

INPUT SET #2				**H_0 *(m)***	**T (s)**	**α_0**	**H_0/L_0**	**m**
				1.5	**4.78**	**30˚**	**0.042**	**1/50**
	Munk	Komar &Gaughan	Weggel	Kamphuis	Goda	Le Mehaute & Koh	CEM	Van Rijn
H_b (m)	1.29	1.60	1.60	0.68	1.17	1.38	1.35	1.22
d_b (m)	1.66	2.05	1.92	1.13	1.50	1.65	1.74	3.04
γb	0.78	0.78	0.83	0.60	0.78	0.83	0.78	0.40
α_b	14.87˚	16.38˚	15.92˚	12.44˚	14.18˚	14.84˚	15.20˚	19.45˚

Table 3.1.C *Results obtained from Input Set #3*

INPUT SET #3				**H_0 *(m)***	**T (s)**	**α_0**	**H_0/L_0**	**m**
				1.5	**4.78**	**0˚**	**0.042**	**1/50**
	Munk	Komar &Gaughan	Weggel	Kamphuis	Goda	Le Mehaute & Koh	CEM	Van Rijn
H_b (m)	1.29	1.58	1.58	0.68	1.17	1.44	1.41	1.29
d_b (m)	1.66	2.03	1.90	1.13	1.50	1.73	1.81	3.22
γb	0.78	0.78	0.83	0.60	0.78	0.83	0.78	0.40
α_b	0˚	0˚	0˚	0˚	0˚	0˚	0˚	0˚

Table 3.1.D *Results obtained from Input Set #4*

INPUT SET #4				**H_0 *(m)***	**T (s)**	**α_0**	**H_0/L_0**	**m**
				1.5	**4.78**	**0˚**	**0.042**	**1/30**
	Munk	Komar &Gaughan	Weggel	Kamphuis	Goda	Le Mehaute & Koh	CEM	Van Rijn
H_b (m)	1.29	1.58	1.58	0.76	1.84	1.55	1.41	1.29
d_b (m)	1.66	2.03	1.80	1.21	2.36	1.71	1.81	3.22
γb	0.78	0.78	0.88	0.63	0.78	0.91	0.78	0.40
α_b	0˚	0˚	0˚	0˚	0˚	0˚	0˚	0˚

Table 3.1.E *Results obtained from Input Set #5*

INPUT SET #5				**H_0 *(m)***	**T (s)**	**α_0**	**H_0/L_0**	**m**
				1.5	**4.78**	**0˚**	**0.042**	**1/100**
	Munk	Komar & Gaughan	Weggel	Kamphuis	Goda	Le Mehaute & Koh	CEM	Van Rijn
H_b (m)	1.29	1.58	1.583	0.63	0.68	1.30	1.41	1.29
d_b (m)	1.66	2.03	1.97	1.09	0.87	1.68	1.81	3.22
γb	0.78	0.78	0.80	0.58	0.78	0.78	0.78	0.40
α_b	0˚	0˚	0˚	0˚	0˚	0˚	0˚	0˚

In the Tables *3.1.A to 3.1.C*, it is observed that breaking wave height and the breaking depth found by expressions of Munk, Goda and Kamphuis do not change with the changes in deep water approach wave angles. Only the angle of breaking changes with changing deep water wave angle since Snell's law is applied for all the expressions to find the breaking wave angle. The most significant changes on the breaking wave parameters with changing deep water approach angle is computed for expressions of Le Mehaute & Koh and CEM (2003), indicating a significant dependence on deep water approach angle.

As the slope is changed with other parameters kept constant, the expressions of Munk, Komar & Gaughan, van Rijn and CEM finds the same breaking wave height and depth in *Tables 3.1.C, 3.1.D and 3.1.E*. The expression of Le Mehaute & Koh (1967) takes into account both the changes in beach slope and deep water wave angles and gives very close results to those of CEM (2003). Breaking wave parameters obtained from breaking expression of Goda show the widest range of change indicating significant dependence on beach slope.

In *Tables 3.1.A to 3.1.E*, it is observed that breaker depth index (γ_b) is different than 0.78, for Weggel, Kamphuis, Le Mehaute & Koh and van Rijn since they use slope dependent breaker indexes except for van Rijn. Van Rijn uses a different breaking point where γ_b=0.40 as explained above. In *Tables 3.1.C to 3.1.E*, where the slope is changed with other input parameters constant, γ_b tends to

increase as the slope gets steep in breaking expressions of Weggel, Kamphuis and Le Mehaute & Koh.

To see the influence of slope on breaking wave characteristics, a set of computations are carried out by using breaking expression of CEM (2003), *Eqn.(3.27)* in which $\gamma_b = 0.72 + 5.6\,m$ given by Collins (1970) instead of $\gamma_b = 0.78$. The results are presented in *Table 3.2*

Table 3.2 *Breaking expression of CEM (2003) with different breaker indexes*

Input Data→	**H_0 *(m)***	**T (s)**	**α_0**	**H_0/L_0**
	1.5	**4.78**	**0˚**	**0.042**
Breaking Parameters		*Expression of CEM with γ_b=0.72+5.6m*		*Expression of CEM with γ_b=0.78*
m=1/100	H_b (m)	1.41		1.41
	d_b (m)	1.82		1.81
	α_b	0˚		0˚
m=1/50	H_b (m)	1.43		1.41
	d_b (m)	1.72		1.81
	α_b	0˚		0˚
m=1/30	H_b (m)	1.45		1.41
	d_b (m)	1.60		1.81
	α_b	0˚		0˚

In *Table 3.2,* it is easily seen that, the results of the two different set of data are quite similar especially for mild slopes and very slightly differ for rather steep slopes. Based on this result, CEM (2003), *Eqn.(3.27)* with breaker depth index of γ_b=0.78 is used in the breaking module of the numerical model. Also results obtained using breaking expression of CEM (2003) lies in between the enveloping curves as seen in *Figure 3.3,* which further supports the decision of implementing Equation 3.2 in the numerical model. Besides, *Eqn. (3.27)* is widely used in

transformation of WIS (Wave Information Study) hindcast estimates to the breaking line, presented in CEM (2003).

Although Weggel (1972) stated the breaker index (γ_b) is 0.78 for flat beaches and increases to more than 1.0 depending on beach slope, seeing the slight difference between the computed values of breaking parameters using *Eqn. (3.27)* with γ_b=0.78 and $\gamma_b = 0.72 + 5.6\,m$ presented in *Table 3.2*, it is acceptable to use γ_b=0.78 with *Eqn (3.27)* given in CEM (2003) within the scope of this study and the numerical model developed herein. However, it may be recommended to include the slope effect in breaker depth index (γ_b) in future studies.

CHAPTER 4

LONGSHORE SEDIMENT TRANSPORT RATE

4.1 Longshore Sediment Transport Concept

Longshore sediment transport rate is the governing parameter which should be comprehended thoroughly in one-line based shoreline evolution, which can be defined as shore parallel movement of the sediment caused by nearshore currents driven by oblique waves, wind and tide. In accordance with one-line theory, cross-shore sediment transport rate onshore and offshore balance each other in long term scale yielding an almost unchanged profile viewed in long term scale. Therefore the spatial variations in the longshore sediment transport rate are considered to lead to changes in the shoreline. In the scope of present study and in the numerical model herein, longshore current is assumed to stem from only oblique breaking waves and longshore currents generated by them, which are dominant in the surf zone.

Any segment of the beach by man-made structures may experience erosion since the hard measures constructed increase the amenity of the beach of concern whereas it may probably cause adverse effects such as recession of shoreline in adjacent beaches. Besides, a lacking design of structure may result in excessive impoundment in the secondary breakwater of a harbor almost closing the entrance gap, jeopardizing the maneuver capabilities through the navigation channel, which was the case in Karaburun fishery harbor (Arı, 2004). The longshore sediment transport is an essential parameter to be assessed as much as accurate since it plays the most significant role whether the shore erodes, accretes or keeps its stability (CEM, 2003).

The transport of sand along the shoreline manifests itself when the drift is blocked by coastal structures such as groins and jetties (Komar, 1977). The updrift side attracts sand and build up a beach due to the barrier whereas the downdrift side experiences erosion resulting from the diffracted breaking wave heights within the sheltered zone of the groin as seen in *Figure 4.1*.

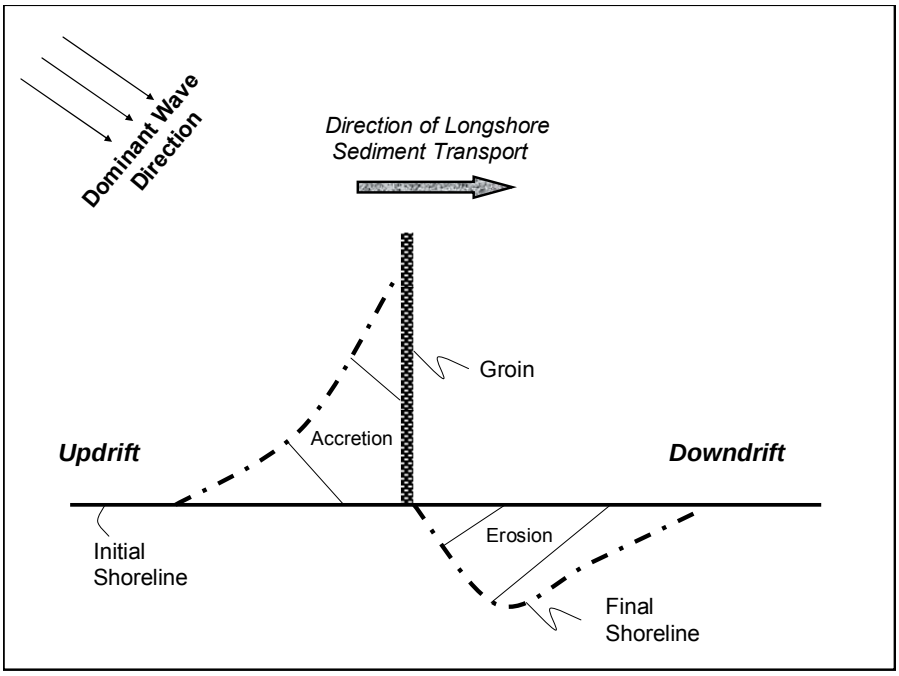

Figure 4.1 *Definition sketch for blockage of longshore transport by a groin.*

As indicated in the introduction part, most of the beaches are eroding, which is an implication of coastal land loss. The causes of erosion are divided into four main groups by Kamphuis (2000) as follows:

- Decrease in sediment supply
- Comminution (Continuous grinding process of sediment by waves)
- Submergence
- Human interference

Kamphuis (2000) states that the beach material formed thousands of years ago by large amounts of river discharge and ice-age glaciers retreat, however large fluctuations in water levels produce the present environmental conditions which form a base for erosion. A good example of substantial reduction of sediment discharged to deltas by rivers owing to the construction of flow regulation structures is expressed in Kökpınar et al. (2005). Submergence takes place caused by the sea level rises basically due to global warming and melting of glaciers being exposed to higher wave action closer to the shore (Kamphuis, 2000).

There are two modes of sediment transport: suspended sediment transport, in which sediment is pushed to move and transported above the bottom by the effect of turbulence caused by breaking waves, and bed-load sediment transport, in which the grains remain close to the bed and move by rolling and saltating. Although this distinction may be made conceptually, it is difficult to separately measure these two modes of transport on prototype beaches (CEM, 2003). Bed load takes place on the sea bottom depending on the bed roughness which is defined as half the ripple height, in Bijker (1971). The suspension transport distribution over the depth of water decays through the bottom to the water level, it is dense just above the sea bed (Kraus et al., 1989). However, bulk sediment expressions calculate the total sediment transport rates.

Some applications may require evaluations of the cross-shore distribution of the transport such as the effective design of groins, jetties, and sand weirs for weir jetties. The maximum local transport has been noted within the shoreward half of the surf zone particularly within the seaward side of this half (CEM, 2003).

The shoreline may be exposed to waves from a variety of directions in which angles between the shore normal and the wave rays approaching from the left are denoted as positive angles (α_R), whereas angles between the shore normal and the wave rays approaching from the left are denoted as negative angles (α_L) in the numerical program as shown in *Figure 4.2*. Wind waves approaching

shoreline can be regarded as waves from the right if they propagate from the right or waves from the left if they come from left as illustrated in *Figure 4.2.* The transport rates to the right, occurring due to the waves coming from the left can be summed up to Q_R, and the transport rates to the left resulting from the waves coming from right can be added to form Q_L. *Eqn. (4.1)* Gross sediment transport rate equals to the sum of the absolute magnitudes of these two rates while the net transport is equal to the difference of these two transport rates and larger of Q_R and Q_L dictates the direction of the net sediment transport rate.

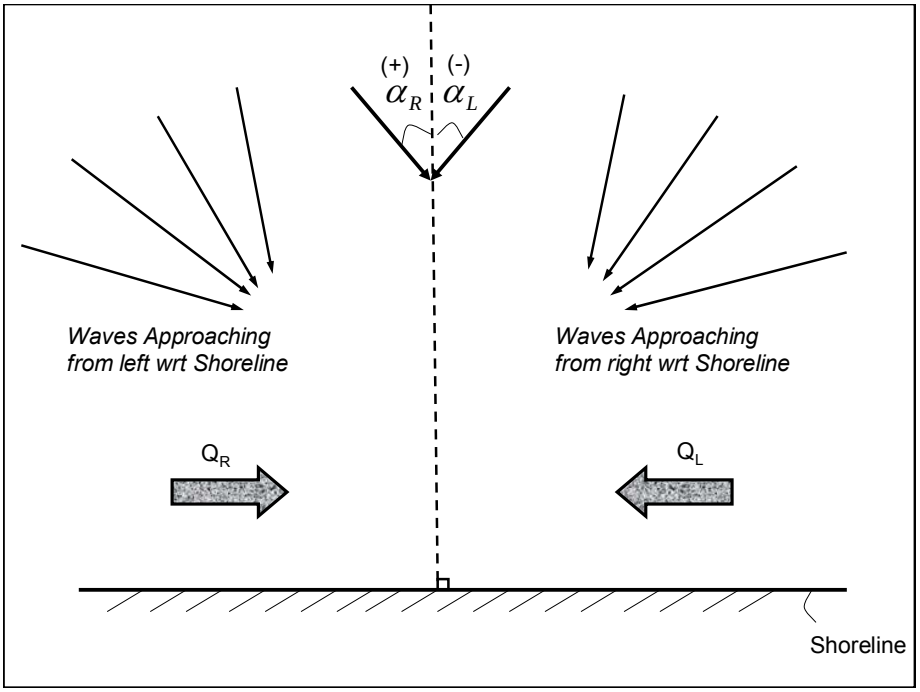

Figure 4.2 *Longshore sediment transport directions*

In general Q_R is denoted as positive and Q_L is regarded as negative.

$$Q_{Gross} = Q_R + |Q_L| \qquad (4.1)$$

$$Q_{Net} = Q_R + Q_L \qquad (4.2)$$

From the points of view of engineering applications, gross transport rate, being irrespective of direction, may be used to estimate the shoaling rates in navigation

channels and uncontrolled inlets whereas the net direction transport indicates the accretion and erosion patterns especially in the vicinity of the coastal structures (CEM, 2003).

Both potential and actual sediment transport rates become more important on beaches with limited sand supply. Potential rate is approached during short periods of time when a large supply of material exist. Kamphuis (2000) gives two examples to comprehend the difference between the actual and the potential transport rates: *(i)* a beach accumulated sediment at actual transport rate during calm climate for years may have eroded out during an important storm, in which there are adequate amounts of sand available for the potential rate to take place. *(ii)* a beach, which formed gradually at the actual rate from the dominant directions may experience the transport at the potential rate immediately when exposed to waves from an unusual direction. These two examples imply that erosion and damage are always very rapid.

Potential transport rates computed by bulk volume expressions do not reflect the actual situation most of the time. Because these expressions are developed by basic assumptions such that (*i)* there are infinite amounts of beach sand to be transported, (*ii)* longshore sediment transport is the net transport and (*iii) t*he effects of individual storms can easily be averaged into long term littoral drift quantities. However, many coastal areas have limited sources of sand. Therefore it is essential to demarcate the potential (computed) sediment transport rate from the actual transport rate. The actual rate is smaller than the potential rate and regarded as a simple fraction of potential rate and it can attained via sediment budget calculations as seen in *Figure 4.3*, which takes into consideration all the sediment inflows and outflows, and all the sediment sources and sinks of the system of concern. (Kamphuis, 2000).

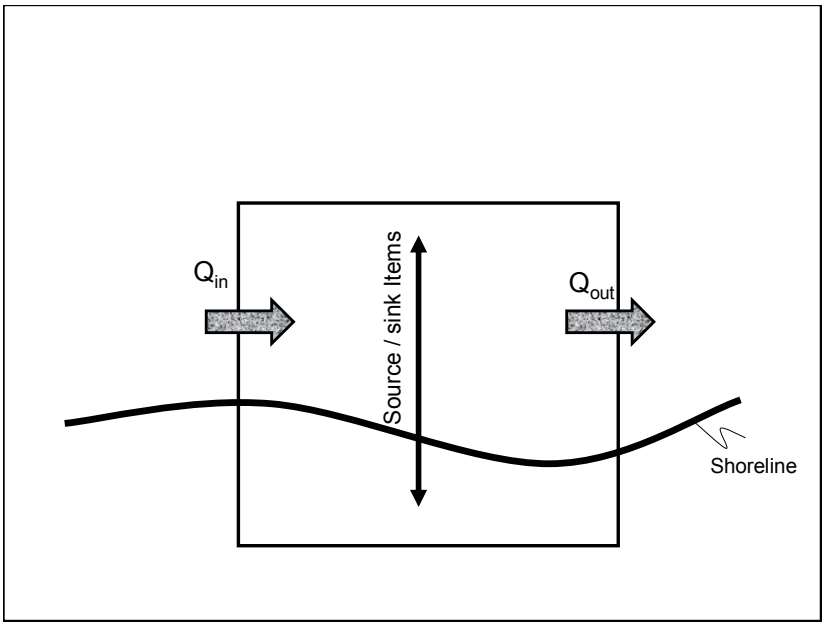

Figure 4.3 *Calculation cell for sediment budget (Kamphuis, 2000)*

A detailed sediment transport calculation covers many carefully measured wave, current, beach and sediment parameters into a numerical model to determine the actual detailed sediment transport rates. The complicated integration of wave, sediment, current and beach parameters and uncertainties inherent in the process lead to bulk volume expressions, which compute the total potential sediment transport rate by using simple wave and beach parameters. (Kamphuis, 2000).

Here, the well-known formula given in Shore Protection Manual (SPM, 1984), Kamphuis (1991) formula and van Rijn (2002) formula for bulk sediment transport rates are going to be referred and compared from the view of applicability to the numerical model and their ability to cover the basic parameters of littoral drift.

4.2 CERC Expression for Sediment Transport Rate

The most common bulk volume expression for sediment transport rate is SPM (1984). The potential sediment transport rate is commonly related with the longshore component of wave power.

$$P_l = \left(E.C_g\right)_b \cdot \sin\alpha_{bs} \cdot \cos\alpha_{bs} \qquad (4.3)$$

where P_l is the longshore component of wave power in (N/sec). E_b is the wave energy calculated from *Eqn. (4.4).*

$$E_b = \frac{\rho g H_b^{\,2}}{8} \qquad (4.4)$$

And C_{gb} is the group velocity in shallow water given by *(Eqn.3.26)*, ρ is the fluid density, g is the gravitational acceleration H_b is breaking wave height, d_b is breaker depth, α_{bs} is the effective breaking angle with respect to shoreline.

$$I_l = K \cdot P_l \qquad (4.5)$$

where I_l is the immersed weight of sediment transport in (N/sec.), K is an empirical dimensionless coefficient. In Komar (1971) K is evaluated as 0.77 empirically based on field data.

$$I_l = 0.28\left(E.C_g\right)_b \cdot \frac{v_l}{u_m} \qquad (4.6)$$

In *Eqn. (4.6),* v_l is a general longshore current velocity which might be due to currents generated with the cell circulation and rip currents, due to tides or winds blowing alongshore as well as to the oblique breaking waves and u_m is the maximum value of orbital velocity in the surf zone.

$$u_m = \left[\frac{2 \cdot E_b}{\rho \cdot d_b}\right] \qquad (4.7)$$

If v_l is generated only by the oblique breaking waves where this is assumed within the scope of this study it is computed from *Eqn. (4.8*) which is proposed by Komar and Inman (1970).

$$v_l = 2.7 \cdot u_m \cdot \sin\alpha_{bs} \cos\alpha_{bs} \qquad (4.8)$$

Substituting *Eqn. (4.8)* into *Eqn. (4.6)* results in *Eqn. (4.5)* is obtained, which is used within this study in accordance with the assumption that longshore current is generated by oblique waves only. If the bulk volume expression is of concern, it is calculated as follows.

$$Q = \frac{K}{(\rho_S - \rho)g(1-n))} P_l \qquad (4.9)$$

where n is the sediment porosity and ρ_S is the density of the sediment. Substituting *Eqn (4.3)* into *Eqn (4.9)* yields the well-known CERC 1984 formula.

$$Q = K.\frac{\rho\sqrt{g}}{(16\gamma^{1/2}(\rho_s - \rho)(1-n)} H_b{}^{5/2} \sin(2\alpha_{bs}) \qquad (4.10)$$

The values of the parameters for use are as follows: ρ_S =2650 kg/m^3, ρ =1025 kg/m^3 for salt water and 1000 kg/m^3 for fresh water, porosity is most commonly assumed as 40% and the breaker depth index γ_b is taken as 0.78.

The calibration of *K* coefficient has been a discussion issue for years and many different values have been proposed ranging from 0.2 to 1.6 (van Rijn, 2002). For the coefficient of *K* a *value of 0.39* is presented in SPM (1984) based on computations utilizing the significant wave height, H_s. Komar (1971) indicates that K decreases with both decreasing energy levels and increasing sediment grain sizes.

To relate the CERC formula with the sediment grain size, del Valle et al., (1993) have presented an empirical formula based on transport rates from aerial photographs of 30 year period shoreline change with use of root mean square wave height, *H,rms*, and given by $H_{rms} = \frac{H_s}{\sqrt{2}}$ where H_s is the significant wave height.

$$K = 1.4 \cdot e^{(-2.5 \cdot D_{50})} \qquad (4.11)$$

where D_{50} is the mean grain size in millimeters *(Eqn. 4.11)* is based on the limited data of the Adra River and valid for D_{50} in the range of 0.4 to 1.5 mm.

A relationship between K and the surf similarity parameter is observed from the laboratory data such that as the type of breaking goes from spilling to plunging, i.e. the surf similarity parameter (ξ_0) increases, K increases as well (Kamphuis and Readshaw, 1978).

4.3 Van Rijn Expression for Sediment Transport Rate

In 2002, van Rijn, has introduced a new engineering methodology for the computation of longshore sediment transport rate in the surf zone of dissipative beaches.

$$Q_{t,mass} = K_1 \cdot (H_b)^{2.5} \cdot V_{wave,L} \qquad (4.12)$$

$$V_{wave,L} = K_2 \cdot (g \cdot H_b)^{0.5} \cdot \sin(2 \cdot \alpha_{bs}) \qquad (4.13)$$

where $Q_{t,mass}$ is the dry mass longshore sediment transport in kg/s, $V_{wave,L}$ is the longshore current velocity similar to the approaches of Bagnold (1963) and Komar (1979) in mid of surf zone due to breaking waves including wind effect, in m/s, H_b is the breaking wave height, and α_{bs} is the effective breaking wave angle.

K_1 and K_2 are coefficients based on computational results of detailed process based cross-shore model of van Rijn (2000) such that $K_1 \cdot K_2 \cdot g^{0.5} \cong 40$,
Substituting (*Eqn 4.13)* into (*Eqn 4.12)* leads to

$$Q_{t,mass} = 40 \cdot (H_b)^3 \cdot \sin(2 \cdot \alpha_{bs}) \text{ in kg/s} \qquad (4.14)$$

Eqn. (4.14) is valid for the range of sand diameters between 0.15 to 0.5 mm, and beach slopes in the range of 1/50 to 1/10. Van Rijn (2002) has used a density of 1600 kg/m^3 of sand grains to obtain the bulk volume expression.

$$Q = 90 \cdot (H_b)^3 \cdot \sin(2 \cdot \alpha_{bs}) \text{ in m}^3\text{/hr} \qquad (4.15)$$

Schoones and Theron (1993) have collected 273 data sets for sediment transport rates from a variety of sites of the world, some of which have been analyzed by van Rijn (2002) to develop a simplified formula for longshore sediment transport rate computations. Since the data set used were scattered to derive a systematic relationships to determine the effects of important parameters and implement their effects in the formula *Eqn (4.15),* a process based cross-shore model is utilized by van Rijn (2000) to make sensitivity computations to see the effects of these parameters such as wave period, particle size, beach slope, profile shape (barred or smooth) and additional longshore velocities other than wave induced longshore current, such as tidal and wind velocities that may move the sediment.

Effect of wave period:

Van Rijn does not include the wave period for wind waves in the formula, however for swell waves a coefficient of $K_{swell}=T_{swell}/T_{ref}$ is introduced to account for the swell wave influence which affects the longshore sediment transport values. Here, van Rijn assumes T_{ref} =6 seconds. For wind waves, this coefficient is not needed to be used in the formula.

Effect of sediment grain size:

To take into consideration the sediment grain size, a similar method in wave period is followed, such that a reference $D_{50,ref}$ is defined as 0.2 mm and again a coefficient of $K_{grain}=D_{50,ref}/D_{50}$ is implemented in the formula with the limitation of $K_{grain,min}=0.1$ for D_{50} , the actual size of grain is greater than 2 mm. This means that the longshore sediment transport of gravel and shingle is assumed to be irrespective of median grain size up to 50 mm. For transport of larger gravels or shingles, a more refined study is to be carried out. This approach additionally lets the computation of longshore sediment transport for coping with erosion problems along gravel and/or shingle beaches which are common along formerly glaciated parts of the world, such as Great Britain Argentina and New Zealand. (Van Rijn, 2002).

Effect of Bed Profile Slope and Shape (Smooth and Barred Profiles):

Bed profile slope is considered to have an influence on the littoral drift, such that the breaking wave heights, thus the longshore sediment transport will be larger on steeper slopes than those on milder slopes. Therefore, van Rijn (2002) has assigned a correction $K_{slope}=\left(m/m_{ref}\right)^{0.5}$ factor where, m_{ref} is the reference slope based on the specific field applications with a value of 0.01 and m is the actual bed slope between the waterline and seaward contour of outer breaker bar. The correction factor K_{slope} is bounded between the values of 0.75 and 1.25.

Bed profile shape also may differ from site to site, such as barred profile with bars on the profile, or smooth profile without major ridges and bars on the profile as shown in *Figure 4.4*. Van Rijn (2002) states that a smooth profile causes a more slightly decline of wave height and more homogenous distribution of longshore sediment transport in which the longshore current loses its peaked tendency compared to a barred profile, therefore, with all the other parameters kept constant, in case of a smooth profile rather than a barred profile, longshore sediment transport rate may substantially reduce up to 50%.

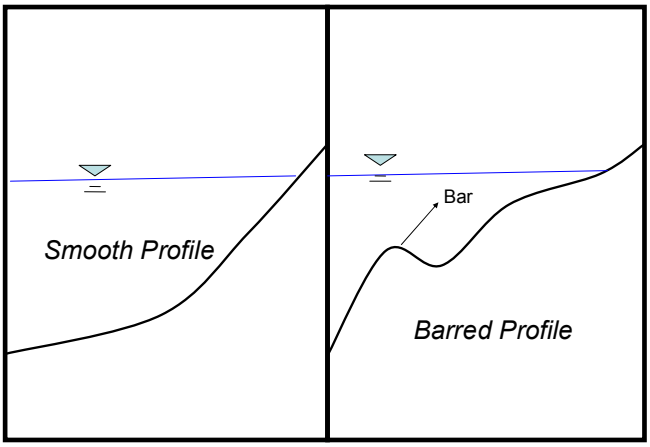

Figure 4.4 *Smooth and barred profiles*

Effect Of Additional Velocities Other Than Wave Induced Longshore Current:

In the scope of this thesis work, the term longshore current is attributed to longshore current generated by the oblique breaking waves. It should be mentioned that wind and tide also induces longshore currents additionally, where wind-driven currents usually exist in the nearshore zone for oblique wind directions and micro-tide is widely efficient at various coastal zones, effects of which should not be ignored and implemented in a more refined study van Rijn (2002). In tidal regions, additional tidal velocity is effective and constitutes up to 50% of the total longshore velocity on Van Rijn's (2002) model results for small wave incidence angles (5˚ -10˚) since the wave induced longshore current is weak relatively for a small angle of incidence. This effect disappears as the wave incidence angle gets larger than 20˚, especially for storm conditions where the breaking waves are dominant. It should be remarked that, wind induced current may have a pronounced value in storm conditions (van Rijn, 2002).

For these reasons, van Rijn (2002) introduced an effective longshore velocity

$$V_{eff,L} = \left[\left(V_{wave,L} \right)^2 + \left(V_{tide,L} \right)^2 \right]^{0.5} \qquad (4.16)$$

where $V_{tide,L}$ is the longshore velocity in the mid surf zone due to tide, and wind effect is included together with wave induced current in the term $V_{wave,L}$, given by *(Eqn. 4.13)*

After the discussions of these parameters included, the *Eqn (4.15)* changes into

$$Q = 90 \cdot K_{swell} \cdot K_{grain} \cdot K_{slope} \cdot (H_b)^{2.5} \cdot V_{eff,L} \text{ in m}^3/\text{hr} \qquad (4.17)$$

Eqn. (4.17) can be used to predict the longshore transport rate in existence of waves normal to the shoreline, i.e. deep water approach angle, α_0 is equal to 0, however with use of *Eqn. (4.15),* the longshore sediment transport rate equals to *0 for* deep water approach angle α_0 is equal to 0.

In future studies, in coastal zones where the tidal effects play an important role, *Eqn. (4.17)* could be used in the developed numerical model.

Van Rijn (2002) gives good discussions about the parameters of the longshore sediment transport rate formula. However, since van Rijn (2002) states that the formula given in *Eqn. (4.17)* is based on the measurements of a specific Egmond site in Netherlands and does not include the wave period for wind waves, only two formulae; CERC and Kamphuis for computation of longshore sediment transport rate are discussed and compared to be used in the numerical model.

4.4 Kamphuis Expression for Sediment Transport Rate

Kamphuis (1991) has also developed a volume bulk expression for longshore sediment transport based on 3-D hydraulic model tests with regular and irregular waves. By non-dimensionalisation of related sediment transport parameters in addition to simultaneously measured wave heights at deep water and through the surf zone, breaking wave angles, longshore current velocity distribution, bed load and suspended load distributions in the experiments lead to a more refined

sediment transport formula which covers wave steepness, wave breaking angle beach slope and relative grain size. Longshore sand transport rate (Q) according to Kamphius formulation in m^3/hour is given as

$$Q = 6.4 \cdot 10^4 \cdot H_b{}^2 \cdot T^{1.5} \cdot m^{0.75} \cdot D_{50}^{-0.25} \cdot (\sin 2\alpha_{bs})^{0.6} \quad \text{in m}^3\text{/year} \qquad (4.18)$$

$$Q = 7.3 \cdot H_b^2 \cdot T^{1.5} \cdot m^{0.75} \cdot D_{50}^{-0.25} \cdot (\sin 2\alpha_{bs})^{0.6} \quad \text{in m}^3\text{/hr} \qquad (4.19)$$

where H_b is the breaker height, T is the significant wave period, m is the beach slope at the particular location where breaking occurs. D_{50} is the median grain size diameter of the sediment, α_{bs} is the efficient wave approach angle during breaking. It is seen that Kamphuis's longshore sediment transport rate expression is proportional to $H_b{}^2$ and $(\sin 2\alpha_{bs})^{0.6}$ both of which tend to correct the overestimating trend of CERC expression, *Eqn. (4.10)* which is criticized particularly for major storms (Kamphuis, 2000). Expression of Kamphuis is an recently accepted formula which is used widely since it covers the important parameters such as wave period, grain size and beach slope.

4.5 Comparison of Expressions and Discussion of Results

After having reviewed the longshore sediment transport rate formulae, using the same set of wave data and sediment characteristics a case study was carried out to compare the formula of CERC (1984), *Eqn. (4.10)* and Kamphuis (1991), *Eqn. (4.19)* in order to see the results in the numerical model. Breaking formula of CEM (2003), *Eqn. (3.27*) is used for computing breaking parameters to calculate both longshore sediment transport formulae.

In the simulation, a case study in which Bafra, Kızılırmak Delta is subject to coastal erosion, given in more detail by Şafak (2006) is presented in order to compare longshore transport rates. In this case study, there are two Y-shaped

groins and an I-shaped groin which are placed at eastern coast of Bafra Delta as seen in *Figure 4.5*

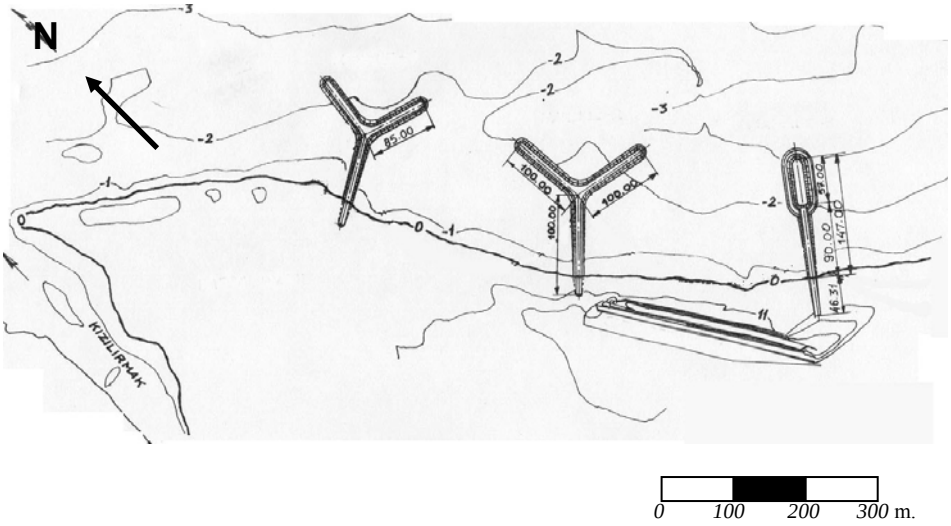

Figure 4.5 *Plan view of Eastern coast of Bafra Delta and the coastal structures*

The shoreline before the structures constructed and the shoreline after 4 years the structures implemented into eastern side of Bafra Delta are measured by State Hydraulic Works (DSI) and obtained to be used in this case study. Y-shaped groins are introduced as T-shaped groins which are interpreted as a combination of an I-groin and an offshore breakwater in the numerical model to be able to use the diffraction patterns developed for T-shaped groins. It is assumed that introducing Y-shaped groins as T-shaped groins would make similar influence on the interaction of wind waves and the structures. The wave input data for the numerical model is given in *Table 4.1*. The diffraction patterns of T-groins are briefly explained in Chapter 5.

Hourly average wind data sets are converted to independent storms and using these storm data together with fetch distances for each direction, wave data

statistics are obtained and significant wave heights versus exceeding probabilities are plotted in *Figure 4.6* (Şafak, 2006).

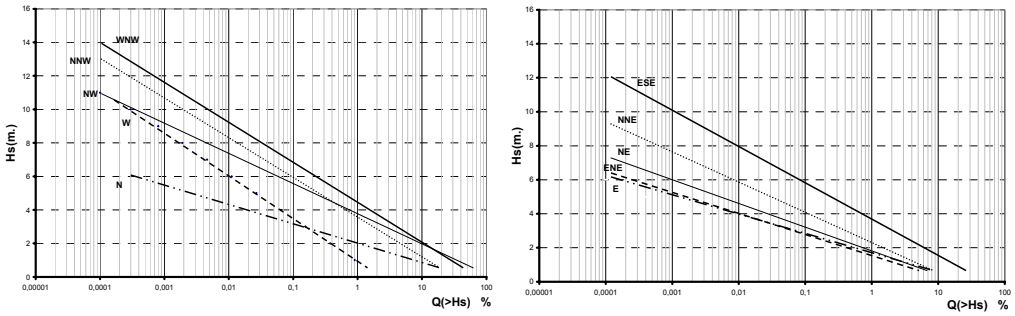

(a) ***(b)***

Figure 4.6 *Probability distribution of deep water significant wave heights*

Then for each direction separately, average deep water significant wave height $(H_{s,0})$ is computed as (Güler ,1997 ; Güler et al.,1998):

$$H_{s,0} = \frac{\sum (P_i . H_i)}{\sum P_i} \qquad (4.20)$$

where H_i is the wave height and P_i is the occurrence probability of wave with height H_i. By this way, annual wave data are obtained.

Table 4 1 Annual average wave heights and corresponding periods

	H (m.)	T (sec.)	f (hrs.)
WNW	1,53	4,83	1365
NW	1,26	4,40	1798
NNW	1,53	4,83	507
N	0,99	3,89	562
NNE	1,24	4,35	185
NE	1,07	4,05	134
ENE	1,01	3,93	114
E	0,98	3,87	151
ESE	1,37	4,57	746

The numerical model results obtained by using CERC expression and Kamphuis expression are plotted together with the measured field data in *Figure 4.7*

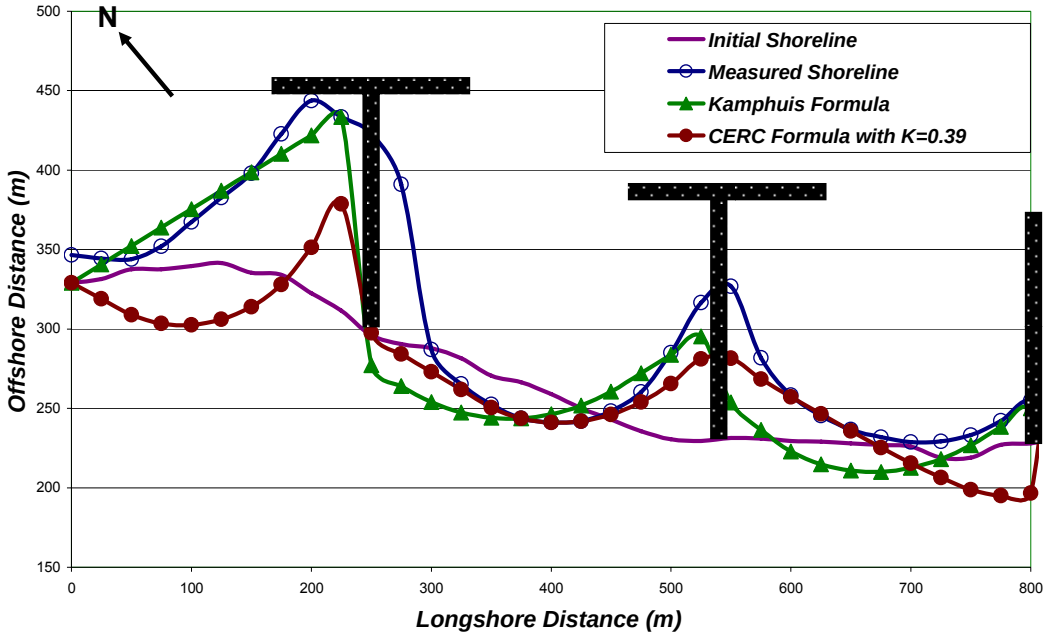

Figure 4.7 *Comparison of longshore sediment transport rate formulae for Eastern coast of Bafra Delta*

As seen from the *Figure 4.7,* the shoreline change computed from the numerical model results using Kamphuis's expression is qualitatively in good agreement with field measurements whereas results obtained from CERC expression with the recommended value of 0.39 for calibration coefficient *K* for significant wave heights, show a different trend of shoreline change which behaves different than the measured field data.

Using CERC expression with the calibration coefficient *K* given by del Valle et al. (1993) *Eqn. (4.11)*, which is valid for grain size in the range from 0.4 to 1.5 mm,

is not applicable to Bafra case study since in Bafra Region median grain size is given as 0.23 mm.

Kamphuis (1991) recommended a calibration coefficient *K* value of 0.12 for CERC expression. In *Figure 4.8* the numerical model results using Kamphuis's expression is compared with that of CERC for *K* equals to 0.12 together with the measured field data.

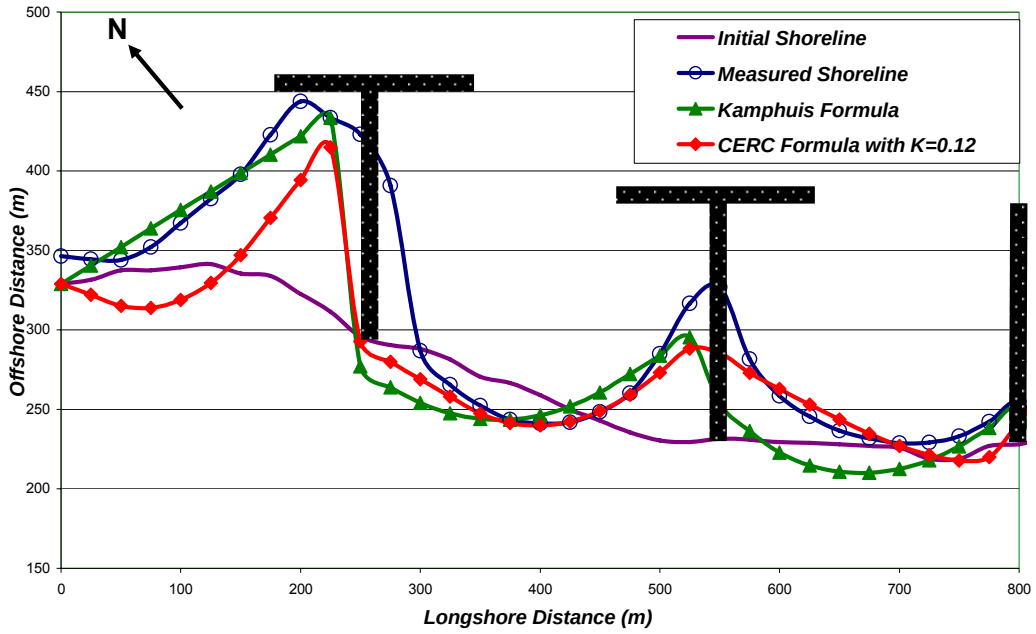

Figure 4.8 *Comparison of Kamphuis expression with CERC for K=0.12*

The qualitative agreement with Kamphuis's expression, *Eqn (4.19)* is also caught for the same site, Bafra Delta with K=0.12 in the CERC expression which is recommended by Kamphuis (1991). The value of calibration coefficient in CERC expression has still an ambiguity with a wide range from 0.2 to 1.6 in the literature. It is noted that, despite the fact that the general trend *K* coefficient is inversely proportion with the grain size, the uncertainties inherent in the relationship still keep due to limited data set and coefficients may vary remarkably for specific sites (CEM, 2003).

Bodge and Dean (1987) state that longshore sediment transport should be related to the breaker type. In Smith, et al. (2004), measured longshore sediment transport rates are compared with those of predicted by the bulk expressions of CERC (1984) and Kamphuis (1991). The recommended K-value of 0.39 for significant wave heights is used in the CERC formula *(Eqn 4.10)* with a porosity of 40 percent. CERC formula seems not to match with the measured values owing to the independency of the expression from the breaker type and thus the wave period.

Results computed from Kamphuis expression give more consistent results with the measured data. This good agreement in predicted and measured values are attributed to the inclusion of wave steepness thus the wave period in *Eqn. (4.19)*, which affects the breaker type as well (Smith et al., 2004).

Under the light of above given discussions, Kamphuis's formula *Eqn. (4.19)* is selected to use in the numerical model, since the result of the simulation for shoreline change obtained using Kamphuis formula matched well with the measured data as seen in *Figure 4.7.* Besides, Kamphuis formula directly includes the wave period, the grain size as well as the beach slope.

CHAPTER 5

COASTAL STRUCTURES IN THE NUMERICAL MODEL

5.1 Offshore Breakwaters

Offshore breakwaters are one of the frequently applied hard measures for coastal stabilization, which are generally constructed parallel to the shoreline. Offshore breakwaters may be divided into two groups depending on their crest heights with respect to mean water level such that if their crests extend above mean sea level, they are denoted as emergent breakwaters; else they are called submerged offshore breakwaters.

Although offshore breakwaters are expensive to build and maintain, in some places where groins and seawalls are not effective for coastal protection, their use has been increased in a great deal recently (Suh & Dalrymple, 1987).

5.1.1. Literature Survey

Hanson & Kraus (1991) give four advantageous properties of offshore breakwaters different than groins.

1. The main purpose of building such an offshore structure is sheltering by reducing the wave energy in the lee of the structure and thus decreasing the sand transport rate behind the structure which let a beach develop as a result increasing the amenity of that segment of beach.

2. Offshore breakwaters have a weakening effect on longshore sediment transport behind their lees, but they do not drive it offshore.

3. Unless a tombolo, morphological shape of shoreline which touches the structure, does not form, the longshore sediment transport rate is not fully blocked which implies the protection of the lee of the offshore breakwater without stopping the alongshore sediment transport rate to downdrift beaches which reduces erosion compared to a groin case.

4. Besides, offshore breakwaters do not let sediment loss offshore by acting as an obstacle for sediments having the tendency to move offshore. If the sandy beaches, especially which have limited source of sediment, are exposed to steep waves having the tendency of transporting sand offshore and if there are no compensating counterpart of swell waves to bring sand back onshore, an offshore breakwater is a much more serviceable measure of coastal defense for that site compared to other alternatives.

The breaking wave heights, and hence the sea levels in the lee of the structure are lower than those outside the shadow zone of the offshore breakwater. Therefore due to the variations at water surface, the longshore currents are directed into the shadow zone of the structure from both ends of the offshore breakwater as shown in *Figure 5.1*

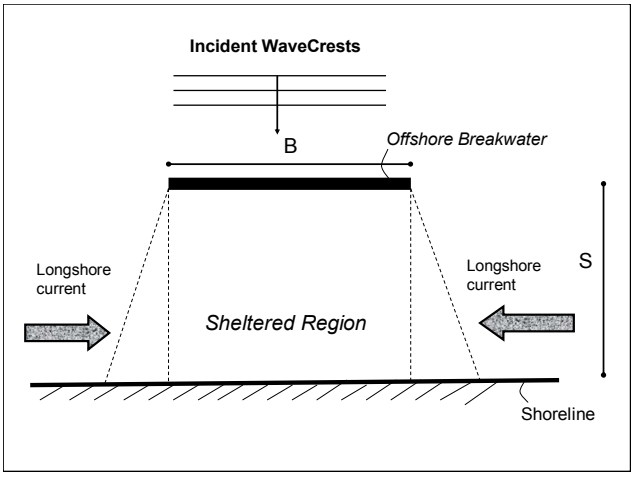

Figure 5.1 *Directions of longshore currents behind the offshore breakwater*

In *Figure 5.1*, *B* is denoted as the length of the offshore breakwater and *S* is the distance between the shoreline and the offshore breakwater.

The main reason for reduction of wave heights, thus the wave energy within the sheltered zone of the structure is the wave diffraction. Waves reaching the structure diffract from both ends and they penetrate into the sheltered zone of the structure. These waves break at an angle to the shoreline and thus transport sand towards the centerline of the structure (Hsu & Silvester, 1990).

The longshore currents transport sand from the adjacent beaches towards the lee of the structure causing accretion behind the structure and erosion in the adjacent beaches. Periodic artificial nourishment may be required for these locations starting from the construction stage as it is the case in groins and jetties. Because, anytime you block or slow down the littoral drift, accretion occurs in a particular strip, but it causes erosion elsewhere, which conforms to the conservation of total beach material.

It is known that the currents generated by breaking waves behind the breakwater accrete sediment in the sheltered area to create a morphological form called a salient (Suh & Dalrymple, 1987). Salients are desired beach planforms formed after constructing offshore breakwaters, since they do not block longshore sand transport completely and protecting the beach behind the structure (Hanson & Kraus, 1991).

Initially double peak salients may form as seen in *Figure 5.2* which is the shoreline configuration with dashed line, but with sufficient wave duration and sediment supply, single peak salient (final shoreline configuration in solid line in *Figure 5.2*) will develop (Hsu & Silvester, 1990).

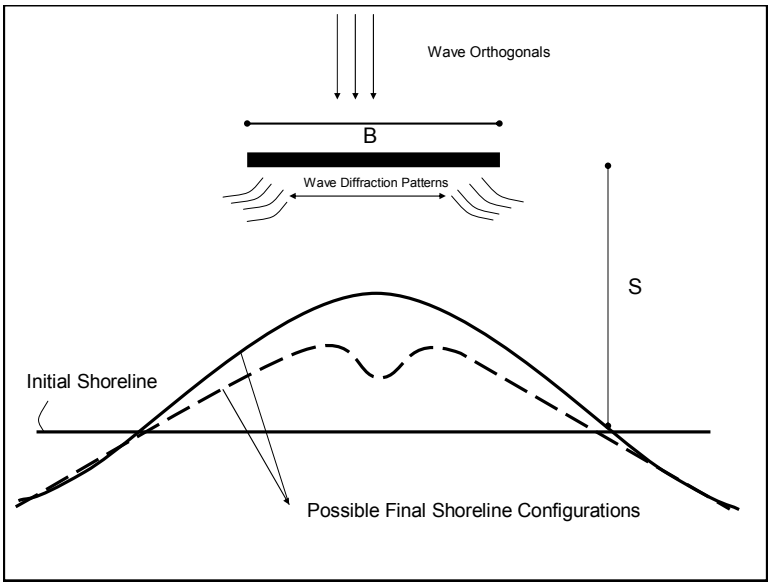

Figure 5.2 *Salient formations responsive to normal incidence*

Nearshore currents meet and generate an offshore current towards the breakwater, and this offshore current separates and generates rip currents offshore and also gradually change the double peak salient into a single one (Suh & Dalrymple, 1987).

In case of oblique incident waves to the breakwater, the wave induced sediment transport tends to decrease at the part of the sheltered zone where the waves are approaching with respect to centerline of the offshore breakwater. Therefore, the apex of the salient occurs at that location which is closer to the tip of the breakwater where the waves are incoming presented in McCormick (1993), as can be seen in *Figure 5.3.*

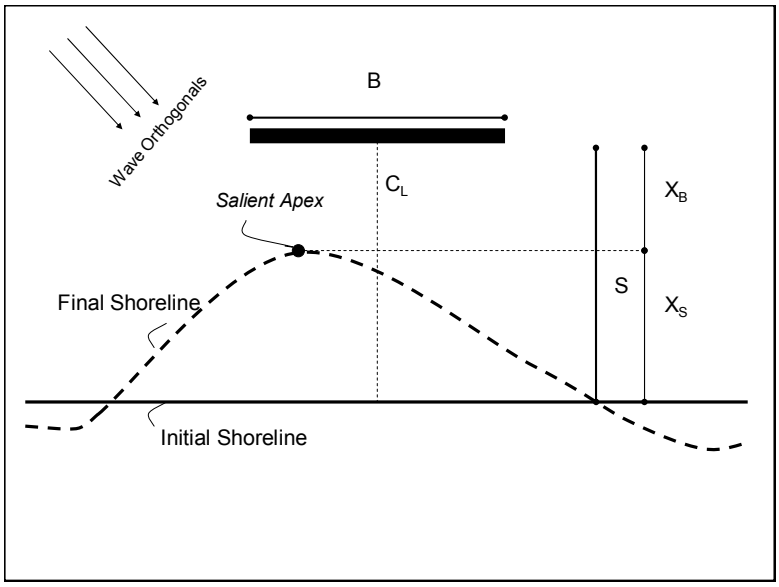

Figure 5.3 *Shoreline response to oblique waves behind an offshore breakwater*

C_L is the virtual centerline which passes through the midpoint of the offshore breakwater, X_S is the distance between the shoreline and the salient apex, which is seaward end of the salient and X_B is the distance between the offshore breakwater and salient apex in *Figure 5.3.*

Tombolo is a special salient which touches the structure. It is generally an undesirable form of beach and response of shoreline to the offshore structure, since tombolo acts as a groin by interrupting the littoral drift and lead to eroding downdrift beaches. In most cases, a tombolo is interpreted as an indication of over-design errors by the team responsible for the structure and the possibility of formation of a tombolo jeopardizes the serviceability of the offshore breakwater (Black, 2003). However, in some cases offshore breakwaters with tombolo offer the advantage that inspection and maintenance are performed more easily compared to the offshore breakwaters which do not have solid connection to the shore (CETN, 1984).

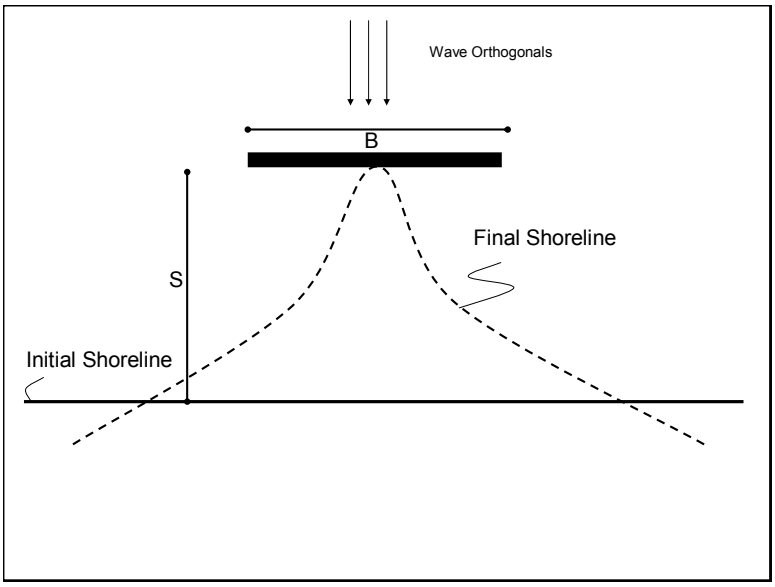

Figure 5.4 *Definition sketch for tombolo formation*

A structure should only be built once the physical system is well understood; otherwise the structure is just a "*full-scale experiment*". The point that the system is permanently altered by any hard structures and the sand formations in their lee should always be kept in mind and predictive tools should be utilized for feasibility (Black, 2003).

5.1.2 Empirical Studies

Many researchers have worked on the shoreline response behind offshore breakwaters. Empirical studies have been made and empirical formulae have been developed in order to predict the shoreline in a rapid and efficient way as a first estimate of salient sizes for engineering use.

Researchers worked on empirical analyses of the shoreline response are, Suh & Dalrymple (1987), Hsu & Silvester (1990), Mc McCormick (1993), Dabees (2000), Ming & Chiew (2000) and Black & Andrews (2001). Dabees (2000) and Black & Andrews (2001) held the same geometric parameters like Hsu & Silvester (1990) taking into consideration the two geometric features of the structures; the length of the structure *(B)* and its distance offshore *(S)*. They have

resulted in empirical formulas, which will be discussed below, for calculating the apex of the salient similar to the one proposed by Hsu & Silvester (1990). Suh & Dalrymple (1987) have developed empirical relationships for single and multiple offshore breakwaters, using again the geometric variables of the offshore structure. They tried to indicate the effectiveness of the offshore breakwater with its volume sand deposition. They have also worked on the effect of surf zone width on sand trapping capacity. Ming & Chiew (2000) has developed an experimental study, which proposes a criterion to distinguish between the formation of a tombolo and that of a salient. On the other hand, McCormick (1993) has included the wave steepness and beach slope in his empirical study as well as the length and offshore distance of the breakwater for single and multiple offshore breakwaters. Waves are allowed to approach from any direction in his study.

5.1.2.1 Empirical Studies on Single Offshore Breakwaters

Hsu & Silvester (1990) have come out with an empirical formula based on the data from a large number of field and laboratory measurements and numerical experiments for normally incident waves.

$$\frac{X_B}{B} = 0.6874 \cdot \left(\frac{B}{S}\right)^{-1.2148} \qquad (5.1)$$

where

X_B: The distance between salient apex and the offshore breakwater

B: The length of the offshore breakwater

S: The seaward distance of offshore breakwater from the shoreline

Hsu & Silvester (1990) reduced the number of many variables affecting the shoreline response to the two most important ones, length of the detached breakwater *(B)* and its distance offshore *(S)*. They concluded in limiting conditions of tombolo and zero salient formation according to the values of ratios

of breakwater length to its distance offshore. Between these two extremities, the extent of salient accumulation exist in equilibrium state, by giving long enough wave duration in model and numerical experiments. For a value of X_B/B=0, i.e. tombolo formation, *B/S* is found to be 5.208. Between values of *B/S*=1.33 and *B/S*=5 natural salients may form, but after long wave duration tombolo formation may be expected. For *B/S*=5, no salient formation i.e. null response is observed.

Dabees (2000) has developed the empirical formula together with his numerical experiment results for validation of his results. His relationship is very similar to that of Hsu & Silvester (1990).

$$\frac{X_B}{B} = 0.645 \cdot \left(\frac{B}{S}\right)^{-1.3507} \qquad (5.2)$$

Ming & Chiew (2000) have brought a boundary ratio for length of breakwater *(B)* to its distance offshore *(S)* between salient and tombolo formations. The boundary value is *B/S*=1.25. In ratios exceeding this value, tombolos tend to happen, whereas salient shapes are met at lower ratios of *B/S*.

Suh & Dalrymple (1987) have observed in the experiment data that *B/S* values between 2 and 3 lead to desirable salient formations, which have sufficient sand trapping capacity. Also they express that if the breakwater is not so far away from the shoreline, for *B/S*>=1, usually a tombolo forms with sufficiently long time.

Black & Andrews (2001) developed an empirical formula, as well.

$$\frac{X_B}{B} = 0.498 \cdot \left(\frac{B}{S}\right)^{-1.268} \qquad (5.3)$$

$$\frac{X_S}{D_{TOT}} = 0.125 \pm 0.20 \qquad (5.4)$$

where

D_{TOT} is the total length of shoreline affected

To summarize the results of these empirical studies, the limits for tombolo and salient formations are presented in *Table 5.1* for the mentioned studies above.

Table 5.1 *Summary of empirical studies by other researchers*

Empirical Limits for Types of Shoreline Responses for Single Offshore Breakwater			
	B/S Ratio for Null Response	*B/S* Ratio for Salient	*B/S* Ratio for Tombolo
Suh & Dalrymple (1987)		<1	>=1
Hsu & Silvester (1990)	~0.2	1.33 - 5	5.208
Ming & Chiew (2000)		<1.25	>1.25
Black & Andrews (2001)		<2	>=2

In his study, Black (2003) also expresses the ratio of breakwater length to distance offshore (*B/S*) should be in the range 0.25-0.5 for optimal benefit with minimal volume and construction costs.

There is neither an explicit method for deciding the dimensions and the ratio of the dimensions for offshore breakwaters for beach protection yet, nor a common point reached among the researchers. Below there are two citations from two different authors, which exemplifies this situation.

The closer the breakwater to the shoreline, the more efficient is the breakwater at sand trapping for the same value of *B/S* value (Suh & Dalrymple, 1987). The optimum protection provided by an offshore breakwater near a shore is a

misconception since in this case problems of accelerating longshore currents in the surf zone and local scour between the reef and the beach occurs causing the compression of the longshore currents (Black, 2003).

For large values of *B/S* i.e. the length of breakwater is much greater than its distance offshore, tombolos may appear. Apart from this ratio, the distance of breakwater from the shoreline is an important design parameter. S should not be so close to and so far away from the shoreline, regardless of the *B/S* values. Because a tombolo is very likely to happen in case of closer breakwaters to shoreline, whereas in the case of much farther breakwaters from the shoreline, offshore structures lose their feature of reducing wave energy and protecting the segment of beach in their lee, which concludes with a null response or minor salients. None of these beach planforms are generally desirable planforms. But as specified above, for specific sites, tombolos might have been intended to act as a groin.

While offshore structures have been built for coastal protection, a thorough understanding of salient formation and structure impacts is needed to prevent over-design and negative impacts in the aesthetic and amenity values of the coast (Black, 2003).

5.1.2.2 Empirical Studies on Multiple Offshore Breakwaters

If a large strip of sandy beach is to be protected, a series of offshore breakwaters multiple (segmented) offshore breakwaters can be constructed (Suh & Dalrymple, 1987).

In this case the length of the breakwater *(B)* and its distance offshore *(S)* are important parameters, and again Suh & Dalrymple (1987) taken the values of *B/S* between 2 and 3 is taken as expressed above in the single breakwater case. Different than single offshore breakwater case, here the gap distance *(G)* between the offshore breakwaters plays an important role on sand trapping phenomenon. As the gap distance gets bigger, breakwaters tend to behave independently like

single breakwaters, which is not the intended case by constructing the segmented breakwaters, whereas if the gap distance is too small the erosion behind the gap is so small and following growth of salient may also be very ignorable (Suh & Dalrymple, 1987).

And a possible shoreline configuration under the effect of multiple offshore breakwaters is given in *Figure 5.5* where salients developed behind the offshore breakwaters and erosion of shoreline occurs behind the gap between the breakwaters in accordance with the results of the laboratory work of Suh & Dalrymple.

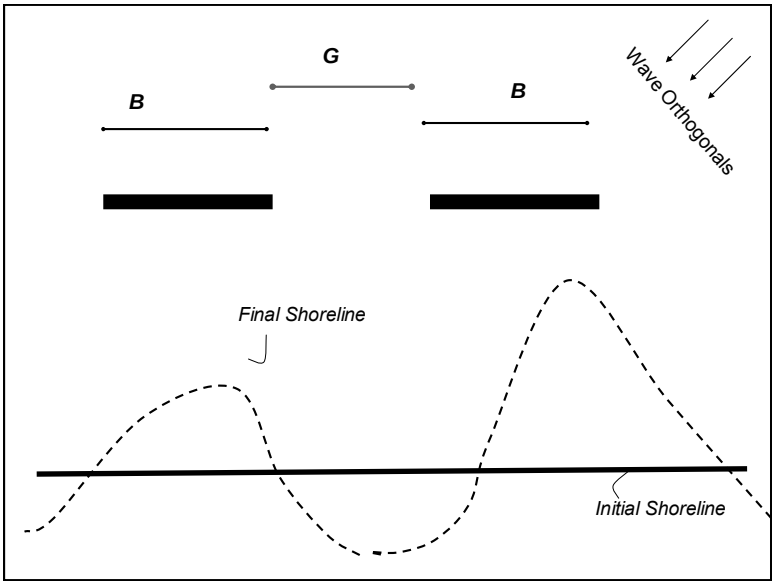

Figure 5.5 *Shoreline change in case of multiple offshore breakwaters*

Suh & Dalrymple (1987) have also developed an empirical formula to find the salient amplitude by using the spacing between breakwaters *(G),* the length of the breakwater *(B)* and its distance offshore *(S*).

$$X_S = 14.8 \cdot \left(\frac{G \cdot S}{B^2} \right) \cdot e^{\left[\left(-2.83 \cdot \left(\frac{G \cdot S}{B^2} \right)^{1/2} \right) \right]} \qquad (5.5)$$

Suh & Dalrymple (1987) states that $G \cdot S/B^2$ appears to be an important for demarcating the tombolo formation from salient formation behind the offshore structure. For values of ($G \cdot S/B^2$) around 0.5, tombolos are expected to form. As this value increases, the salient amplitude decreases.

In CETN (1991), *Eqn. (5.5)* was applied to various segmented offshore projects. In the article it is concluded that, this relationship tends to overpredict the furthest seaward point of the salient for the majority of prototype data evaluated; but, appears to accurately predict for pocket-beach type structures with periodic tombolo formations.

Seiji, Uda, and Tanaka (1987) predict the following gap erosion relationships, where gap erosion is defined as the retreat of shoreline to the lee of the gap from the initial (pre-project) shoreline position. The expressions of Seiji et al. (1987) are presented below.

For	$\frac{G}{S} < 0.8$	no erosion at gap	*(5.6)*
For	$0.8 \le \frac{G}{S} \le 1.3$	possible erosion at gap	*(5.7)*
For	$\frac{G}{S} \ge 1.3$	certain erosion at gap	*(5.8)*

These expressions were evaluated for the prototype data and *Eqn. (5.8)*, the no erosion expression is stated that it gives results which are in good agreement with the measured field data (CETN, 1991).

Equations (5.5) through *(5.8)* may serve as fast and efficient pre-design parameters for multiple offshore breakwaters, and can be more valuable if these parameters are supported by the field or laboratory measurements in similar wave, currents, and sediment regimes.

An understanding of the nearshore sediment transport regime and pre-project sediment budget is essential before the design together with the experience collected from field measurements (CETN, 1984).

5.1.3 Development of Numerical Model for Offshore Breakwaters

Based on the assumptions and limitations of one-line theory, which has already been introduced in Chapter 2, offshore breakwater module of the numerical model is developed, regarding that the diffraction patterns at the tips of the breakwater are the major agent which affect and modify the breaking wave heights and breaking wave angles. Wave transmission through the breakwater which is thought to result from either by wave overtopping and direct transmission is also considered to change the breaking wave heights and angles behind offshore breakwaters. Wave reflection in front of the structures is neglected within the scope of this study and the numerical model developed.

High construction cost and the difficulty in predicting the response of the shoreline are the two main disadvantages of offshore breakwaters, as Hanson & Kraus indicated in 1991. To diminish the latter disadvantage, there are strong tools such as field and laboratory studies and numerical experiments. Numerical models of shoreline evolution aids the understanding of the shoreline evolution phenomenon qualitatively, predicts the long-term future evolution, and assesses the effects of planned construction and activities.

Input data required by the model is as follows. Firstly, the number of offshore structures that will be used in the simulation is required. Then for each of the offshore structure, the longshore location of the offshore breakwater, the length of the breakwater *(B)*, its distance offshore, *(S)* and the wave transmission coefficients of each breakwater are all entered by the user as the input values about structure geometry and structure features.

Small amplitude linear wave theory assumptions and equations are applied for refraction and shoaling of incident waves as they come closer to the shoreline.

Shoaling and refraction computations are done according to the *Eqn. (3.1)* and *Eqn. (3.2),* respectively.

5.1.3.1 Diffraction Computations for Single Breakwaters

For diffraction computations behind offshore breakwaters, two methods based on the same principle will be used, both of which will be outlined below. The principle is that diffraction computations are performed through the directional spreading of the incident waves (Goda, 1985). In this respect, it is assumed that an obstruction blocks out a portion of incoming directional wave spectrum (Kamphuis, 2000).

Firstly, Kamphuis's (2000) regression analysis for diffraction values according to the angle θ, which is the angle between the shadow line of the structure and the related point at the line of breaking *(Figure 5.6)*, is utilized to compute diffraction coefficients. Then Leont'yev's (1999) expressions will be presented which is based on Goda's (1985) diffraction principle. The shadow zone and the angle θ are illustrated in *Figure 5.6*. The pragmatic expressions of Kamphuis (2000) for diffraction behind structures are as follows;

$$K_d = 0.71 - 0.0093\theta + 0.000025\theta^2 \qquad \text{For } 0 \geq \theta \geq -90 \qquad (5.9)$$

$$K_d = 0.71 + 0.37\sin\theta \qquad \text{For } 40 \geq \theta > 0 \qquad (5.10)$$

$$K_d = 0.83 + 0.17\sin\theta \qquad \text{For } 90 \geq \theta > 40 \qquad (5.11)$$

where K_d is the diffraction coefficient, and θ is the angle in degrees between the shadow line of the structure and the related point at the line of breaking

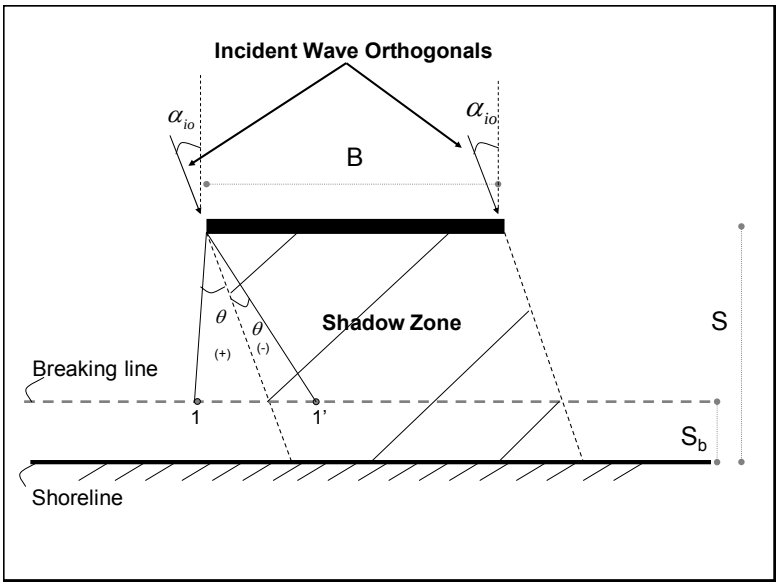

Figure 5.6 *Definition sketch for angle* θ

In *Figure 5.6* S_b is the length of the surf zone, which is the distance from the shoreline to the breaking line. Leont'yev (1999) assumed an average value of concentrating parameter S_m which characterizes the degree of directional spread based on Goda's (1985) principle in the wave field. A similar regression analysis of Leont'yev (1999) leads to the following equations.

$$K_d = 1 \qquad \text{for } \theta \le -\pi/6 \qquad (5.12)$$

$$K_d = 0.1 \cdot (\theta + \pi/6) + \cos^3(\theta + \pi/6) \qquad \text{for } -\pi/6 \le \theta \le \pi/2 \qquad (5.13)$$

$$K_d = 0.087(3 - 4\theta/\pi) \qquad \text{for } \pi/2 \le \theta \le 3\pi/4 \qquad (5.14)$$

$$K_d = 0 \qquad \text{for } \theta \ge 3\pi/4 \qquad (5.15)$$

where again K_d is the diffraction coefficient, and θ is the angle between the shadow line of the structure and the related point at the line of breaking. However, Leont'yev (1999) used a different sign convention from Kamphuis (2000) such that angle θ is treated as positive when measured towards the structure, which is the opposite case in *Figure 5.6.*

In both of the methods used in the simulation, the diffraction coefficients from the source points which are located at a distance from the both ends of the offshore breakwater are computed. Concept of transition zone proposed by Dabees (2000) and the concept of sheltered zone are illustrated in *Figure 5.7.*

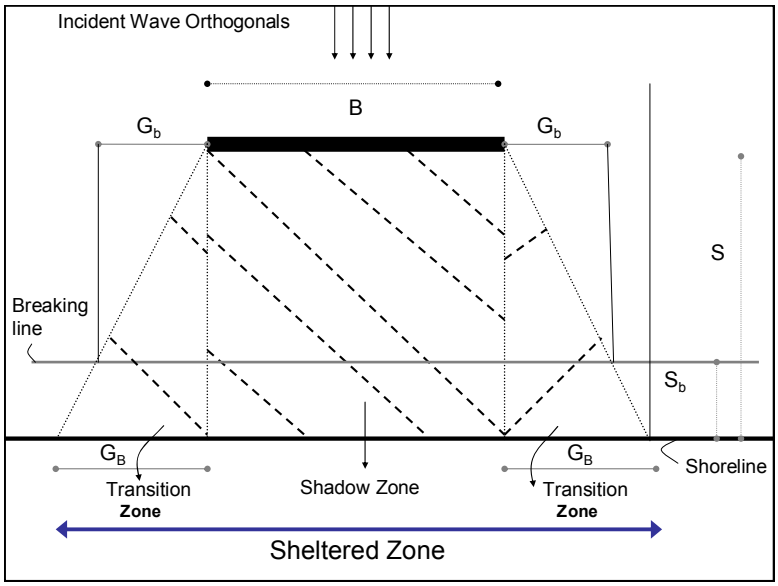

Figure 5.7 *Description of transition and sheltered zones for normal incidence*

$$G_B = 3 \cdot L_{off} \tag{5.16}$$

where, $L_{off\ is}$ wavelength at the depth of offshore breakwater and calculated according to the linear wave theory by refraction and shoaling. G_B is the width of the transition zone, which is assumed approximately 3 times the incident wavelength at the depth of offshore breakwater in Dabees (2000).

$$G_b = G_{B.}\left(\frac{S - Sb}{S}\right) \tag{5.17}$$

where G_b is the width of transition zone on the breaking line, S_b is the distance between the breaking line and shoreline and S is the distance between the breakwater and the shoreline as shown in *Figure 5.7.*

Shadow zone is the region which is bounded by the breakwater, the shoreline and the extension lines of the wave orthogonals up to the shoreline without changing any direction, as illustrated in *Figure 5.7*. Transition zone is the region between the shadow line of the structure and a virtual line drawn from the tip of the breakwater to the shoreline such that the width at the shoreline is 3 times the wavelength at the depth of offshore breakwater. Both of the transition zones of an offshore breakwater for normal incident wind waves are shown in *Figure 5.7.*

Sheltered zone is segment of shoreline which is between the transition zones of the structure from both of the tips of the structure as seen in *Figure 5.7.* Sheltered zone of an offshore breakwater includes both of the transition zones of the structure from both of the tips of the structure together with the shadow zone.

The diffraction pattern behind an offshore breakwater through the boundary of the proposed transitional zone is demonstrated and it is compared with the conventional diffraction methodology in *Figure 5.8* as in Dabees (2000).

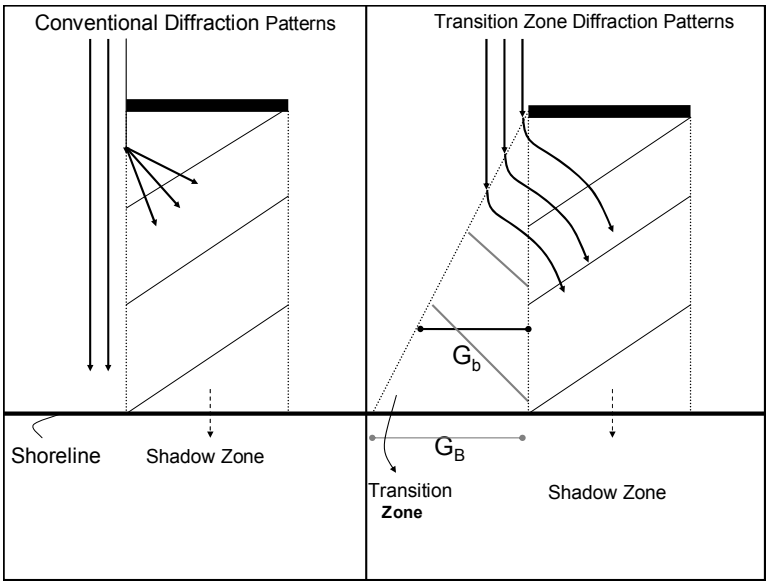

Figure 5.8 *Comparison of transition zone and conventional diffraction patterns (Dabees, 2000)*

It is easily seen in *Figure 5.8* that, taking into account the transition zones wave orthogonals change direction as they enter the transitional zone whereas in the conventional method wave orthogonals change direction if they touch the boundary of the shadow zone of the structure.

The diffraction coefficients computed from the left end of the offshore breakwater is called K_{d1} and the one computed from the right end is called K_{d2} as illustrated in *Figure 5.9*, for the case of normal incidence of wave rays.

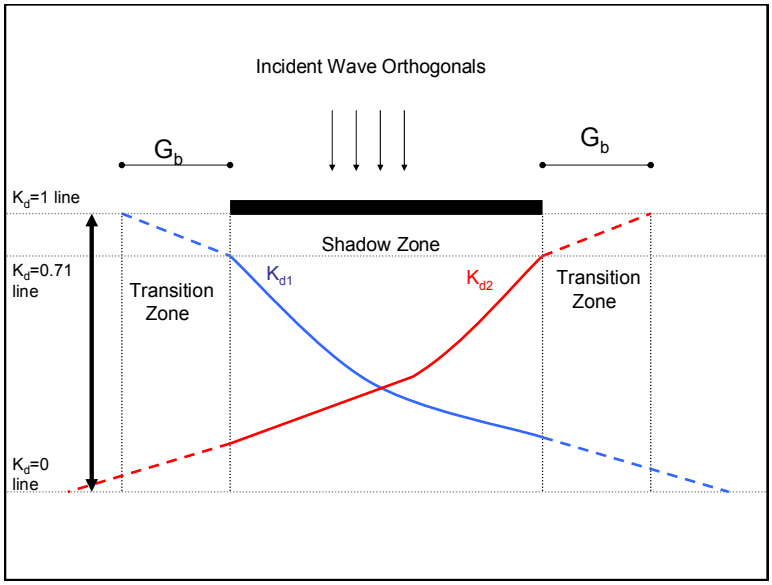

Figure 5.9 *Schematic representations of K_{d1} and K_{d2}*

They are calculated separately along the sheltered zone, and in the shadow lines both K_{d1} and K_{d2} have the computed values of 0.71 on opposite ends as shown in *Figure 5.9.* Because Goda (1985) assumes that the half of the wave energy is lost along the extension of the wave ray at the tip of the breakwater. And from *Eqn.* (4.4), it is known that wave energy is proportional with the square of wave height. Therefore this 50% reduction in wave energy corresponds to approximately 29% in the wave height coming to the structure, which gives 0.71 value of diffraction coefficient along the shadow boundary lines of the structure. And in the numerical model, it is assumed that both of the diffraction coefficients reach unity at the

ends of the transition zones on the breaking line since the offshore structure is supposed to diffract the wave rays within the transition zones and the shadow zone.

In this respect, they are linearly extended to the transition zone grids, by using the difference between the K_d value computed at the shadow zone and 1 divided by distance of transition zone at the breaking location (G_b). Similarly the minimum values of K_{d1} and K_{d2} are calculated at the reverse ends of the breakwater. The minimum values of diffraction coefficients are again linearly extended to 0, by using the difference of the diffraction coefficient computed at the shadow zone grid and the one computed at the adjacent grid. The grids that the coefficients reach 0 do not necessarily need to be the ends of the transition zones.

In *Figure 5.9*, the calculated portions of the diffraction coefficients behind the shadow zone, are in solid line, and the extensions of both coefficients K_{d1} and K_{d2} to both 1 and 0 are displayed in dashed lines. These assumptions are applied in the numerical model developed.

As seen in *Figure 5.9*, from the beginning of the left hand side transition zone to the end of the right hand side transition zone, there are two diffraction coefficients, K_{d1} and K_{d2} which are computed along the sheltered zone. To calculate the longshore sediment transport rate along this corridor, an integrated diffraction coefficient is required.

Since the directional spectrum of Goda (1985) is considered, simple summation of K_{d1} and K_{d2} will overestimate K_d values, which results inaccurate predictions of salient amplitudes. Therefore, a procedure is developed such that wherever K_{d1} or K_{d2} has a larger value than the other, the integrated K_d value will be equal to the larger one. This procedure is also illustrated in *Figure 5.10*, which is actually an upper portion of *Figure 5.9.* This assumption is also used in the numerical model.

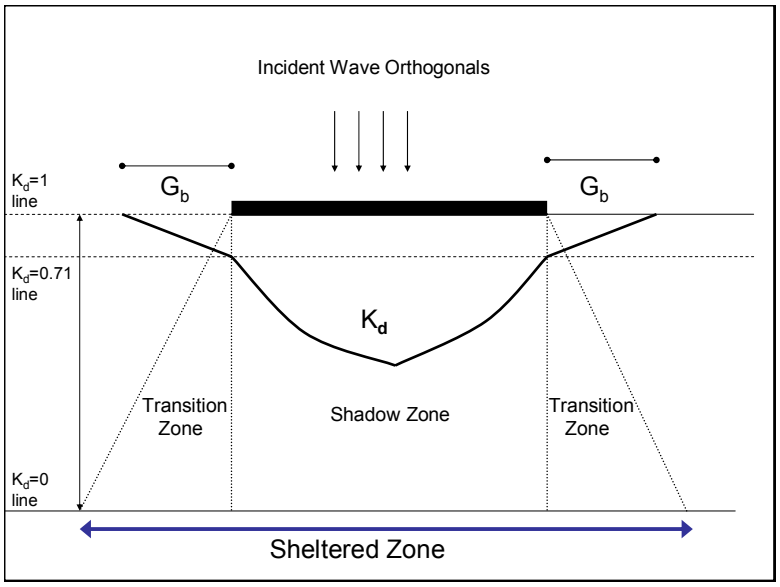

Figure 5.10 *Schematic representation of diffraction coefficient,* K_d behind offshore breakwaters

The diffraction coefficients computed from the left end of the offshore breakwater K_{d1} and the one computed from the right end K_{d2} will be integrated as explained above and shown in *Figures 5.9* and *5.10 in Figure.* In order to compute K_{d1} and K_{d2}, two regression analyses for diffraction coefficients, Kamphuis (2000) through *Equations.* (*5.9)* to *(5.11)* and that of Leont'yev's (1999) through *Equations* (*5.12)* to *(5.15)* were mentioned above based on Goda's directional spectrum principle.

To decide on which methodology is going to be utilized in the numerical model, a sample run is carried out with input wave data of significant deep water wave height $H_{s,0}$=1.5 m, T_s=4.8 seconds and deep water wave approach angle α_0 equals to 0. A shoreline of 5 km is hypothetically given with a 200 m long offshore breakwater at 2400 m distance from the left, and placed 150 m offshore with respect to the initially straight shoreline. The results for the K_d coefficients and the calculated salient sizes are shown graphically below. The difference between the diffraction coefficients computed by the two methods is obvious in *Figure 5.11.*

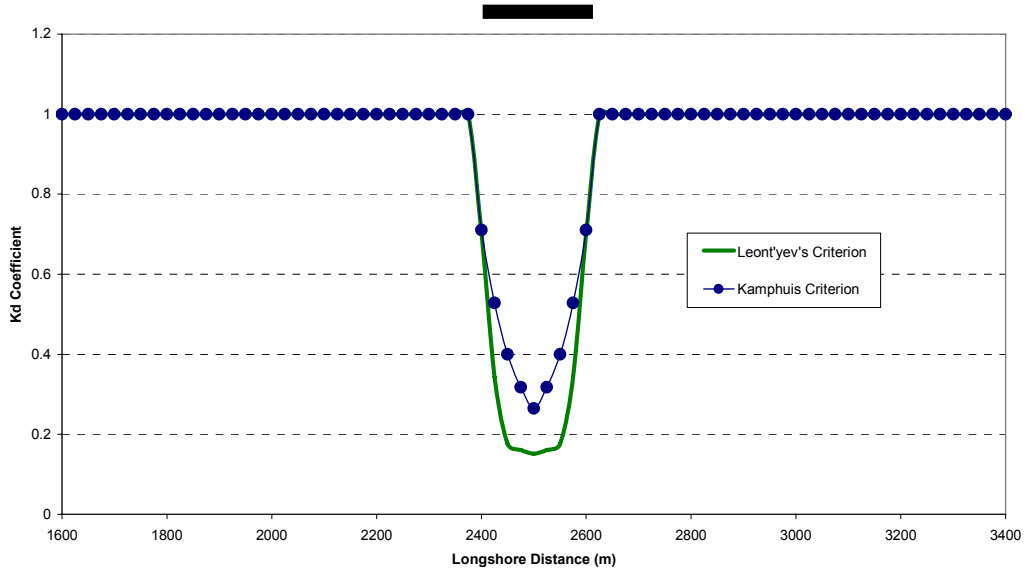

Figure 5.11 *Comparison of computed K_d coefficients by different methods*

In *Figure 5.11* running the model with Leont'yev's regression analysis gives lower K_d values, especially at the mid-grids of the sheltered zone, compared to the ones obtained from Kamphuis's procedure. This leads to smaller wave heights in the lee of the offshore structure and hence lowers longshore sediment transport rates. The end result of this comparison is that, computation of diffraction coefficients using the procedure given by Leont'yev (1999), leads to smaller amplitude salient sizes in short term.

Two sample runs with the same input data of *Figure 5.11* are carried out to compare the salient figures computed by diffraction computation methods of Kamphuis and Leont'yev for t=2500 hours and for t=10000 hours. The results are presented in *Figures 5.12* and *5.13.*

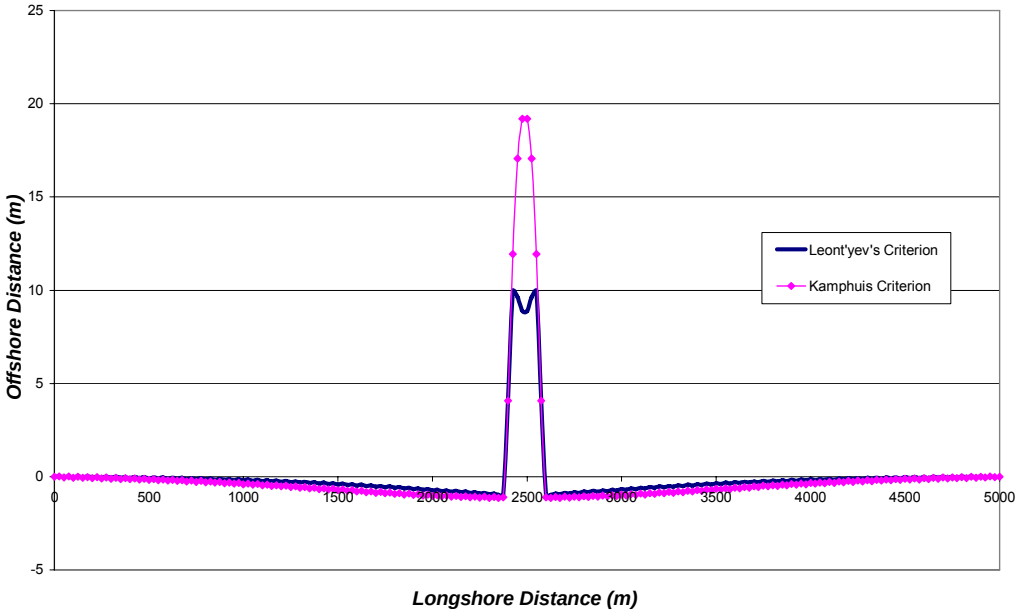

Figure 5.12 *Comparison of shoreline responses by the two diffraction computation methods for t=2500 hours*

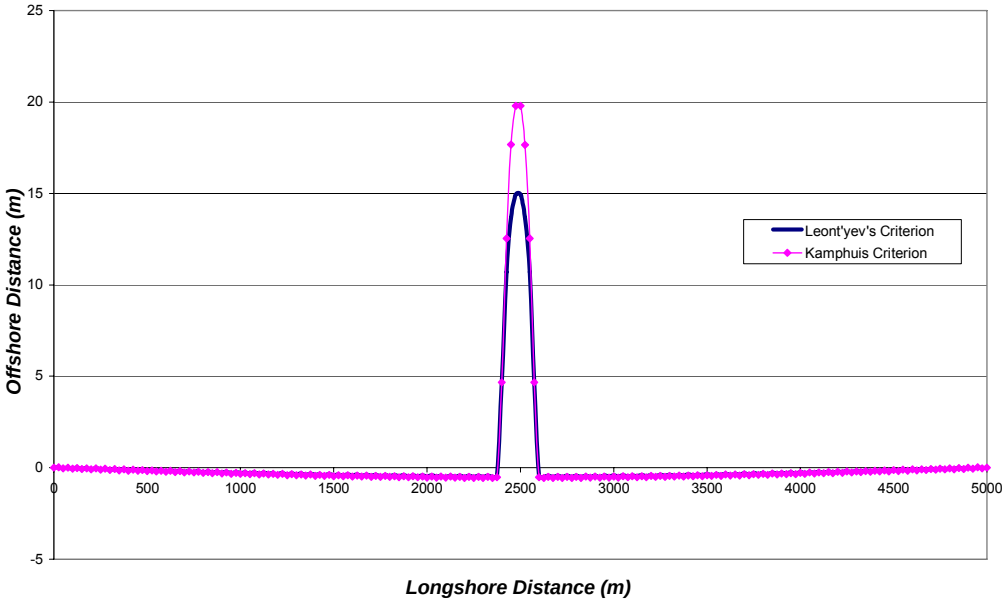

Figure 5.13 *Comparison of shoreline responses by the two diffraction computation methods for t=10000 hours*

As it is seen from *Figure 5.12* and *5.13*, under the same wave action & structure interaction, shoreline changes computed by Leont'yev's diffraction patterns find smaller salient amplitudes when compared to shoreline changes computed by diffraction patterns of Kamphuis. This is because that Leont'yev's methodology has lower diffraction coefficients in the middle of the sheltered zone of the offshore breakwater as seen from *Figure 5.11*, which implies lower breaking wave heights leading to smaller longshore sediment transport rates and shoreline changes.

In *Figure 5.12* salient predicted by Leont'yev's diffraction methodology finds a smaller salient apex than the one predicted by Kamphuis's diffraction methodology for 2500 hours. The difference between the salient sizes tends to decrease for 10000 hours which is presented in *Figure 5.13.*

Both procedures have similar trends, however, diffraction coefficients change gradually from one grid to the adjacent when the procedure given by Kamphuis (2000) is applied in the numerical model, whereas the diffraction coefficients change more rapidly using the expressions of Leont'yev's (1999). Both methodologies contain pragmatic expressions and are not difficult to adapt to the numerical models. Due to the reasons stated above, expressions given by the Kamphuis are used for diffraction computations behind coastal defence structures in the model. It is noted again that the diffraction coefficients are computed along only the shadow zones by this methodology. Outside the shadow zone, coefficients are extended to 0 and 1 in a linear trend which is explained above in detail and illustrated in *Figure.5.9*

After diffraction coefficient, K_d is computed, the breaking heights calculated from *Eqn. (3.27)* as if there were no structures should be modified by multiplying with K_d coefficient.

$$H_{bd} = K_d \cdot H_b \qquad (5.18)$$

where H_{bd} is the modified breaking wave height due to coastal structures, $K_{d\,\text{is}}$ the diffraction coefficient, and H_b is the breaking wave height as if there were no structures or obstructions.

5.1.3.2 Diffraction Computations for Multiple Breakwaters

In order to compute the diffraction coefficients for a multiple offshore breakwater system, the diffraction coefficients (K_d) computed by the above methodology for each offshore breakwater at first. Then, if the sheltered zones of two consecutive offshore breakwaters intersect with one another, the diffraction coefficient of each breakwater is multiplied by the adjacent one to obtain the K_d values at the grids of this intersection region.

As seen from *Figure 5.14*, $K_{d,L}$ is the integrated diffraction coefficient of the breakwater at the left side of the gap and similarly $K_{d,R}$ is the integrated diffraction coefficient of the breakwater at the right side of the gap. To obtain the $K_{d,I}$ which is the K_d coefficient at the grids of the intersection region, *Eqn. (5.19)* is used given by Hanson & Kraus (1991).

$$K_{d,I} = K_{d,L} \cdot K_{d,R} \qquad (5.19)$$

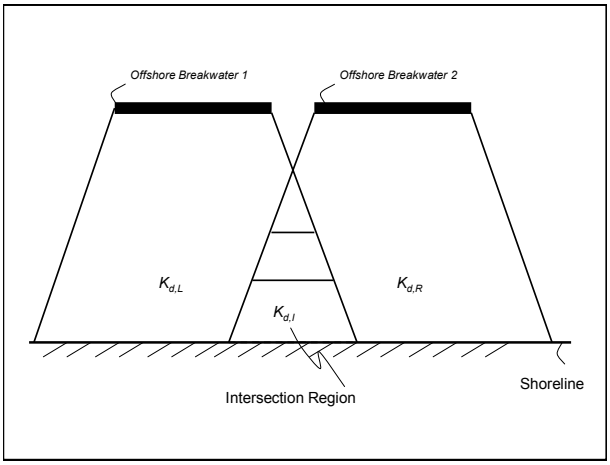

Figure 5.14 *Diffraction behind multiple offshore breakwaters*

Eqn. 5.19 implies that as $K_{d,L}$ and $K_{d,R}$ each approach unity, the total diffraction coefficient, $K_{d,I}$ approaches unity as well. This means a large gap between breakwaters or a pronounced distance from the diffraction sources such that breakwaters behave independently. On the contrary in case there is a small gap between offshore breakwaters, $K_{d,I}$ approaches zero as either $K_{d,L}$ *or* $K_{d,R}$ goes to zero, which is an indication of a location deep inside a wave shadow zone, implying a good protected point (Hanson & Kraus, 1991).

5.1.3.3 Breaking Angle Calculation Scheme

Having determined the methodology for diffraction to be used in the numerical model, the breaking angle calculation scheme is going to be focused on.

In Dabees (2000), concept of transition is explained in detail. In small amplitude linear wave theory, lateral energy transfer, i.e. diffraction starts at the tips of the breakwater and the wave heights are reduced as the wave rays approach the shore radially. Kamphuis and Warner (1987) have developed a minimum radius of curvature limit, which improved the breaking angle and diffracted wave height computations. In this respect, the wave orthogonals do not begin to change direction from the tips of the breakwater, but from the boundary of the transition zone, which was shown in *Figure 5.8*. The wave orthogonals also radially propagate towards the shore in this case, but they start to diffract from a source point I as seen in *Figure 5.15.* Moreover, the path between the source point I and any point at the line of breaking, a symbolic point A, is a circular arc instead of a linear path. According to Dabees (2000), inclusion of transition zone and circular arc path between points I and A in the *Figure 5.15*, prevents larger values for wave heights and angles and hence inaccurate salient sizes particularly for far offshore structures.

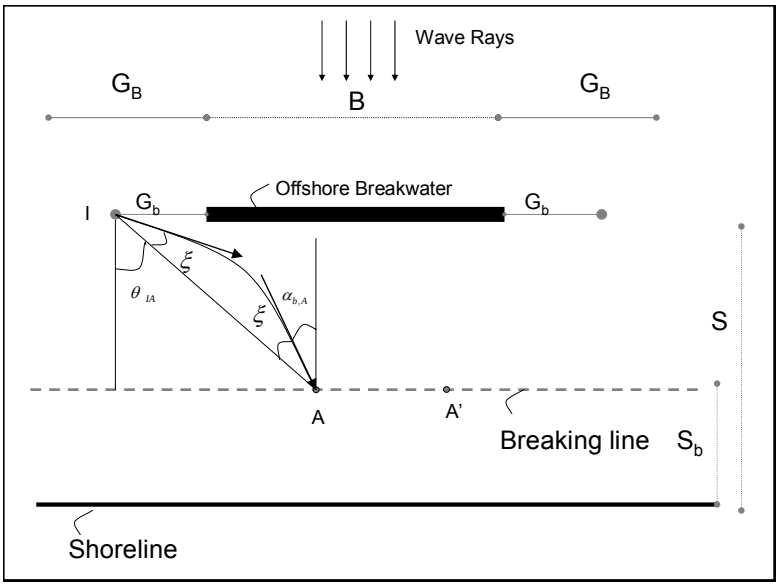

Figure 5.15 *Breaking angles behind offshore structures (Dabees, 2000)*

Applying the Snell's law between points I and A,

$$\frac{\sin \alpha_{b,A}}{\sin \alpha_I} = \frac{L_{b,A}}{L_I} \qquad (5.20)$$

where L_I and $L_{b,A}$ are the wavelengths at points I and A

$$\alpha_{b,A} = \theta_{IA} - \xi \qquad (5.21)$$

where

θ_{IA} is the angle between the vertical and between the straight line points I and A, $\alpha_{b,A}$ is the breaking angle at point A resulting from the source point I at the left tip of the breakwater and ξ is the angle difference between the linear path and the circular path at point A. In Dabees (2000), ξ is approximated as follows

$$\xi = \tan^{-1}\left[\left(\frac{L_I - L_{b,A}}{L_I + L_{b,A}}\right)\tan\theta_{IA}\right] \qquad (5.22)$$

In the simulation, the initial value of the breaker angles due to the source point I at the left of the breakwater are assigned to the initial breaking angle computed from *Eqn. (3.23)*. $\alpha_{b,A}$ angles are calculated along the sheltered zone of the offshore breakwater at the breaking line according to the direction of the littoral transport. Similarly, from the other tip of the offshore structure, the same calculation scheme *Eqn. (5.21)* is followed and $\alpha_{b,A}'$ angles (the breaking angle at point A' due to the source point at the right tip of the breakwater) are calculated for the grids within the sheltered zone.

After having modified wave breaking angles along the sheltered zone of the offshore breakwater, we have two breaking angles $\alpha_{b,A}$ and $\alpha_{b,A}'$ computed by the procedure proposed by Dabees (2000) as explained above. However, in *Eqn. (4.19)* one breaker angle adjusted to shoreline is required to calculate the longshore sediment transport rate at that grid.

In obtaining the breaking angles, the position of the point with respect to tips of the breakwater is important. The breaking angles at a random point are in the dominancy of the closer tip to that point, since the diffraction pattern resulting from the closer tip to that point is highly effective but through the farther tip this effect diminishes. Therefore interpolation is made between $\alpha_{b,A}$ angles computed from the source point at the left of the breakwater and $\alpha_{b,A}'$ angles computed from the source point at the right of the breakwater within the sheltered zone to compute $\alpha_{b,o}$, which is the integrated breaking wave angle behind an offshore breakwater to be used in the longshore sediment transport rate formula.

By this way, the breaking wave angles are calculated in the lee of an offshore breakwater. If there is more than one offshore breakwater, the same procedure is applicable. But if the sheltered zone of each breakwater intersects, the wave angles calculated separately from each breakwater are simply added up in the intersection region illustrated in *Figure 5.14*.

Then the angle of breaking with respect to the shoreline, α_{bs} is calculated from *Eqn (2.1)* to be used in the longshore transport formula in the model

5.1.3.4 Wave Transmission through Offshore Breakwaters in the Numerical Model

Wave transmission through the offshore breakwaters is regarded as the combination of overtopping or direct transmission through the permeable breakwater. Transmission coefficient depends on many variables such as core material, crown height, wave height and period (Hanson & Kraus 1991). Furthermore, wave transmission patterns are affected over different time scales governed by tidal variations and long term changes in water levels (Wamsley et al., 2002).

In the numerical model, a constant transmission coefficient K_t is assumed such that $0 \leq K_t \leq 1$ in which $Kt = 0$ implies no transmission (impermeable and very high crested breakwater i.e. no overtopping) and $Kt = 1$ indicates 100% transmission which is the no breakwater case (Hanson & Kraus 1991).

In the numerical model developed, wave breaking heights and wave breaking angles are calculated by diffraction patterns within the sheltered zone of the offshore breakwater as if the breakwater was impermeable and infinitely high i.e. $Kt = 0$. Then if the breakwater is subject to wave transmission, diffraction coefficients and wave breaking angles are modified as follows given by Dabees (2000).

$$K_{dt} = K_d \cdot (1 - K_t) + K_t \qquad (5.23)$$

$$(\alpha_{b,o})_t = \alpha_{b,o} \cdot (1 - K_t) + \alpha_{b.} K_t \qquad (5.24)$$

where K_{dt} is the modified diffraction coefficient according to the transmission coefficient, K_t and $(\alpha_{b,o})_t$ is the modified breaking angle due to transmission, $\alpha_{b,o}$ is the integrated breaking angle computed without including transmission and $\alpha_{b.}$ is the breaking angle computed by *Eqn. (3.27)* as if the breakwater did not exist.

A degree of submergence can be assigned with a specific value of transmission coefficient. Therefore submerged breakwaters or reefs are also interpreted by the numerical model with a known or estimated coefficient of wave transmission and and their influences on the shoreline are computed.

Sample runs were carried out to test the numerical model for transmissive offshore breakwaters. Through the sample runs wave data input and the structure configuration are held the same, only the transmission coefficients were different. The shoreline is assumed to be initially straight. The results of the runs are presented in *Figures 5.16.*

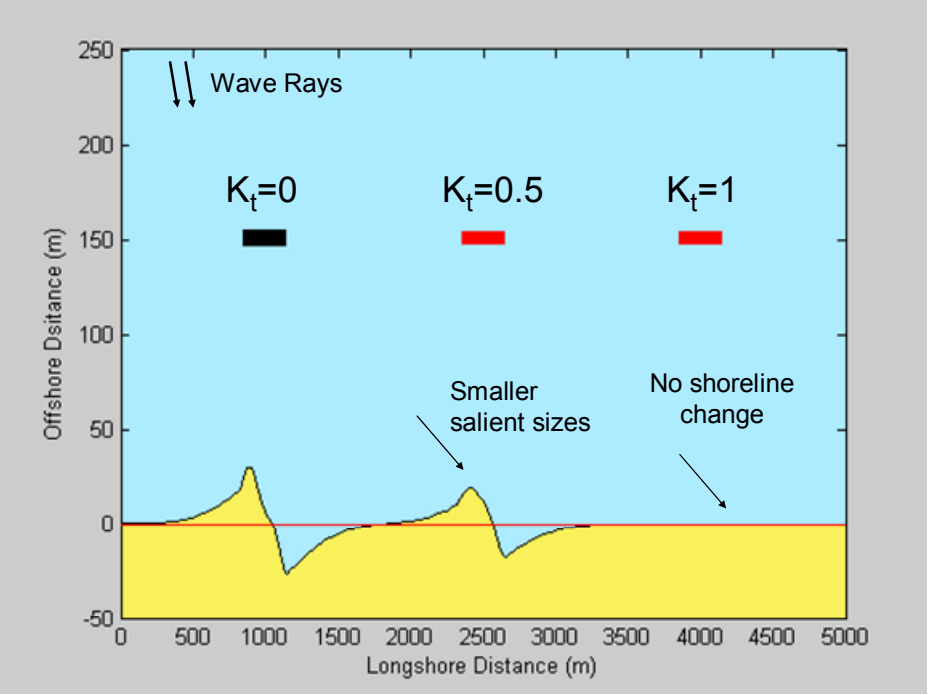

***Figure 5.16**. Shoreline responses for different transmission coefficients*

In *Figure 5.16*, the final computed shoreline configurations are shown and the location of the structure is indicated. It is seen that as the transmission coefficient increases, salient sizes behind the offshore breakwaters decrease which was expected. Also a hypothetical offshore breakwater case with *100% wave* transmissivity i.e. $K_t=1$ is tested to check to sensitivity of the model and it resulted in no influence on the shoreline in the line of expectations.

5.1.4 Model Simulations for Offshore Breakwaters

After having developed the offshore breakwater module of the numerical program, in order to check the model validity, morphological shapes behind the offshore breakwaters given in the literature are compared with those obtained from numerical model herein.

Firstly, a single offshore breakwater which is 400 meters long and placed 150 meters offshore is presented with the same wave input data ($H_{s,0}$=1,5 m. and T_s=4.8 sec.) for different occurrence frequencies in hours and for normally incident waves..

Single peak salients may occur at the earlier time steps, but with sufficient amount of sediment supply and with adequate time double peak salient turns into a single peak salient. The results are presented in Figure 5.17.

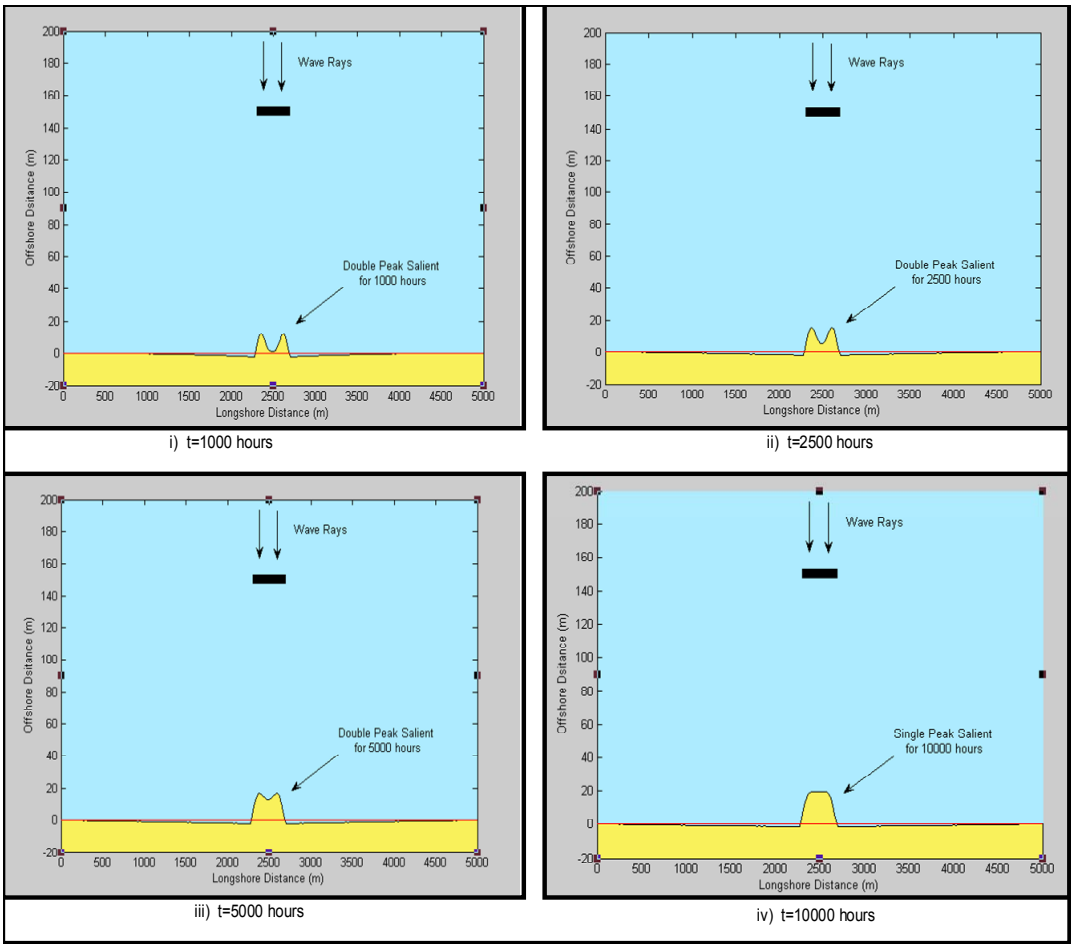

Figure 5.17 *Salient growth with time*

In *Figure 5.17*, it is seen that double peak salient gradually changed into a single peak salient with sufficient time as indicated by Hsu & Silvester (1990). Double peak salient formed after 1000 hours tend to grow for 2500 and 5000 hours of wave action keeping their double peak salient shapes. However, for 10000 hours the transformation from double peak salient into single peak salient occurred.

For oblique wave incidence the farthest seaward end of the salient behind offshore breakwater is closer to the tip, from where the waves are approaching (McCormick, 1993). This situation is tested and the model results are presented in *Figure 5.18.*

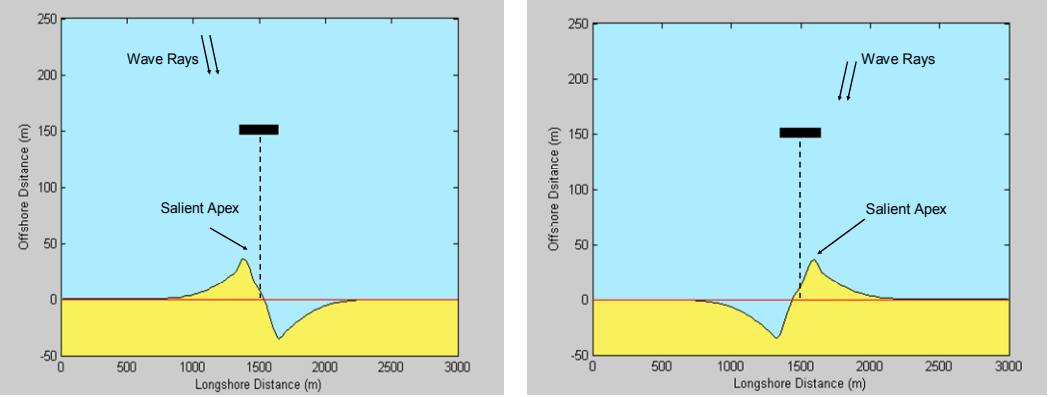

Figure 5.18 *Shoreline responses behind offshore breakwaters under oblique waves*

The numerical model computes the shoreline change in the expected manner under oblique waves such that salient apexes are close to the tip of the breakwater from where the waves are approaching.

And lastly three sample runs have been performed for multiple offshore breakwaters in which shoreline configurations for different gap spacing values between offshore breakwaters are tested. The simulations were carried out for three offshore breakwaters whose lengths and offshore distances are 200 meters and 150 meters respectively. The wave data input was $H_{s,0}$=1.75 m. and T_s=5.17sec.

In the following *Figure 5.19* the gap spacing values *(G)* are 100meters, 300 meters and 400 meters for three sample runs.

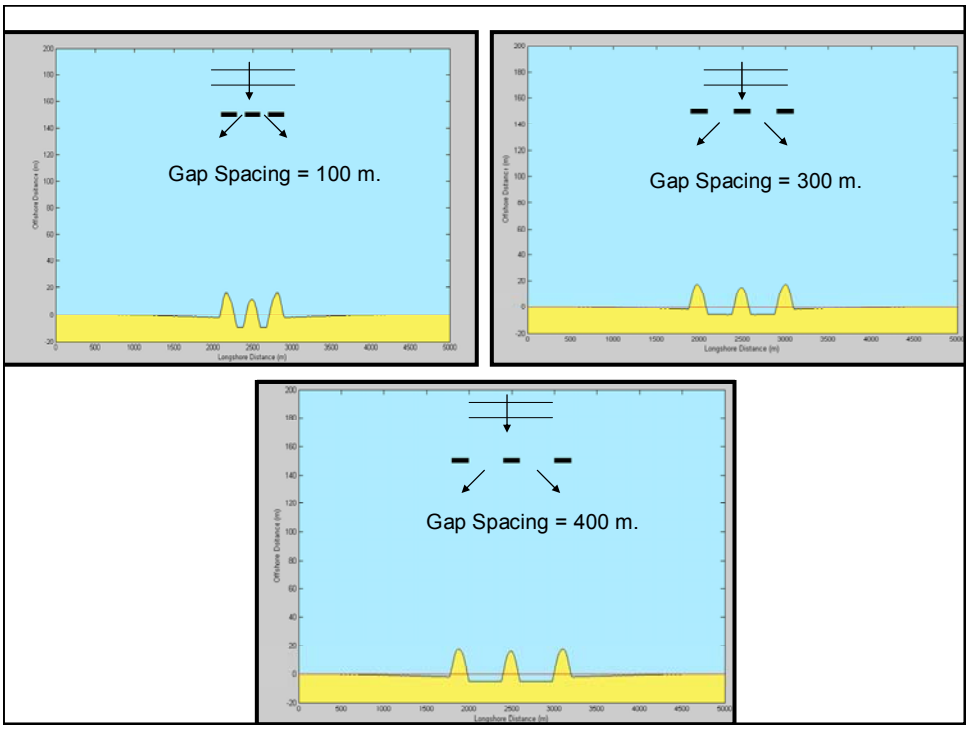

Figure 5.19 *Shoreline changes due to different gap distances*

As *Figure 5.19* is analyzed from left to right and from top to bottom, it is seen that the shoreline change behind three offshore breakwaters with gap spacing, *G=100* m. has smaller but deep erosion patterns. As the gap distance increases to 300 m, a wide strip of beach is eroded behind the gaps but the maximum recession is smaller than that of the case with *G=100* meters. For *G=400* meters this tendency of increased width of erosion but smaller recession increases which implies that the breakwaters almost behave independently such that there is no interaction between them as noted by Suh & Dalrymple (1987). The numerical results presented in *Figure 5.19* shows qualitative similarity with the physical model test results of Suh & Dalrymple (1987).

5.2 Brief Introduction of T-Shaped Groins

In some cases, T groins can be utilized to provide reduction in erosion patterns and smooth transition of shoreline to the adjacent beaches through the downdrift side of longshore sediment transport (Dabees et al., 2004). In the numerical

model, T-shaped groins are introduced as a combination of an offshore breakwater and a groin.

The groin location in this case, could be anywhere on the segment of beach within the sheltered zone of the offshore breakwater behind its lee in order that the numerical model interprets this combination as a T –groin, as seen in F*igure 5.20*. The length of the groin can be up to the distance offshore of the offshore breakwater, or it may shorter.

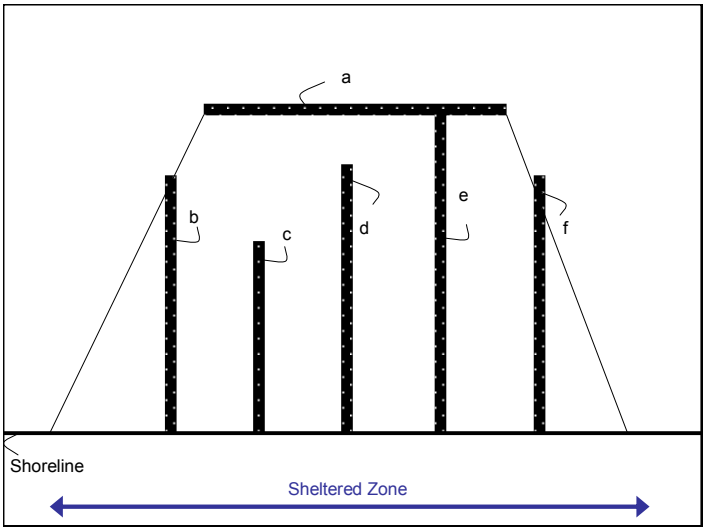

Figure 5.20 Different T-groins interpreted by the numerical model

All the double combinations of the coastal structure elements provided that one of the elements is ‘a’ in *Figure 5.20*, are interpreted as a T-groin for the numerical model. For example ‘a’ and ‘b’ together form a T-groin as well as other elements ‘c’, ’d’, ‘e’ and ‘f’ form with the coastal defence element ‘a’ as shown in *Figure 5.20*.

In the numerical model, wave diffraction patterns modifying wave breaking heights and angles are governed by the location of the groin. Offshore breakwater part of T-groin have the same diffraction manner of a single offshore breakwater as explained in Section 5.1.3.1, whereas the groin part of the T-groin behaves like

a complete barrier. T-groin constraint developed in the model herein is given in more detail in Şafak (2006), where also seawall constraint is included into the model. The boundary conditions of seawalls is that beach backed by a seawall can not move landward of it (Hanson and Kraus, 1986). Groin constraint in which the regression analysis of Kamphuis (2000) for diffraction patterns is given in Baykal (2006) in the numerical model.

Here is a sample run in *Figure 5.21* in which a T-groin and an offshore breakwater is placed in an initially straight shoreline under the same wave climate and beach characteristics.

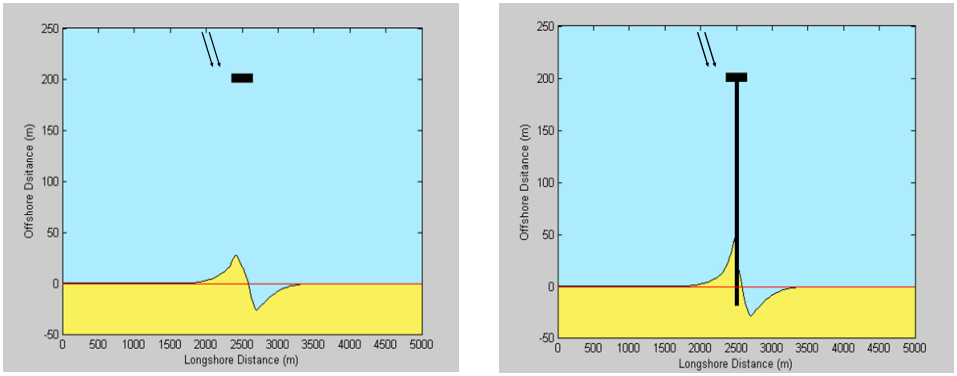

Figure 5.21 *Results of numerical models for offshore breakwater and T-groin*

The accretion at the updrift side of T-groins is slightly larger than that of the offshore breakwater since the groin acts as a complete barrier for sediment. Also the downdrift part of the shoreline recess farther inland in the T-groin case.

CHAPTER 6

COMPARATIVE STUDY WITH AN APPLICATION

In Chapter 5, offshore breakwater constraint of the developed numerical model is explained in detail and T-groin constraint is briefly introduced. In this Chapter, a case study will be referred in Eastern Coast of Bafra Delta where Kızılırmak flows into the Black Sea as seen in *Figure 6.1*. The flow regulation structures built on Kızılırmak River disturbed the sediment budget of the region and led to erosion in the Eastern Coast of Bafra Delta (Kökpınar et al., 2005). Coastal defence structures are built to control the erosion in the region as seen in *Figure 6.2*.

Figure 6.1 *Location of case study*

In *Figure 6.2*, a recent layout of the existing coastal defence structures in the Eastern Coast of Bafra Delta are presented by a picture extracted from Google Earth (2006).

Figure 6.2 *Coastal defence structures in Bafra region (Google Earth, 2006)*

In *Figure 6.2* there are 6 *I-shaped groins* and 2 Y-shaped groins constituting 8 coastal defence structures. If you look landward to the *Figure 6.1*, in the right there are two Y-shaped groins and an I-groin as indicated in the same figure. In the case study the shoreline configurations changed by these three coastal structures are examined in the numerical model by Şafak (2006). The measured shorelines before the structures implemented and after 4 years of period that the structures constructed were obtained from State Hydraulic Works (DSI). The median grain size of the region is given as 0.23 mm.

Y-groins are treated as T-groins in the model as explained in Chapter 4. A qualitatively well matching result between the numerical model developed herein and the final shoreline configuration is achieved. The wave data hindcasting for the region are given by Şafak (2006). This case study is also used in Chapter 4, to decide on which longshore sediment transport formula to be used in the numerical model.

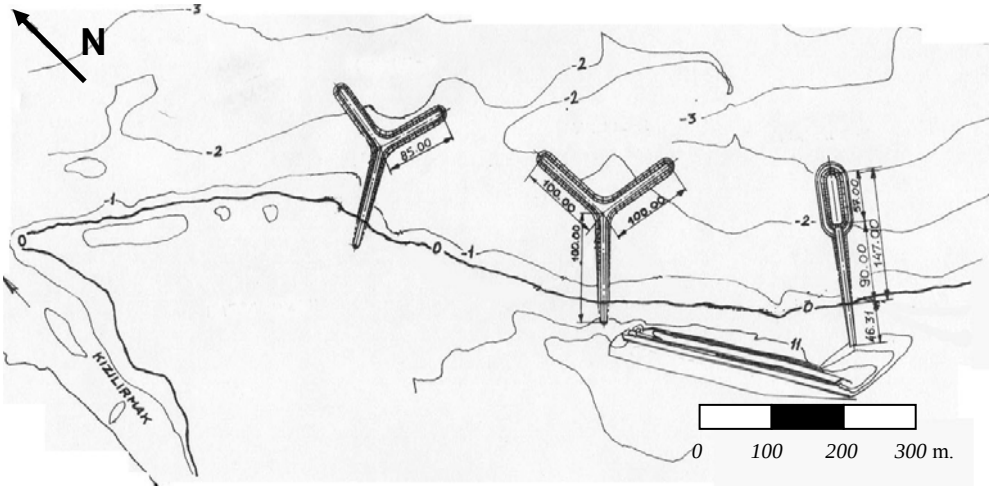

Figure 6.3 *Layout of the existing structures*

It should be noted that *Figure 6.3* and *Table 6.1* were given in Chapter 4. They are given again here for the convenience of the reader to follow the text continuously. The wave data input was presented in Chapter 4.

Table 6. 1. Annual average wave heights and corresponding periods from all directions

	H (m.)	T (sec.)	f (hrs.)
WNW	1,53	4,83	1365
NW	1,26	4,40	1798
NNW	1,53	4,83	507
N	0,99	3,89	562
NNE	1,24	4,35	185
NE	1,07	4,05	134
ENE	1,01	3,93	114
E	0,98	3,87	151
ESE	1,37	4,57	746

The qualitative agreement between the numerical model results and the measured field data for the existing structures are presented in *Figure 6.4.*

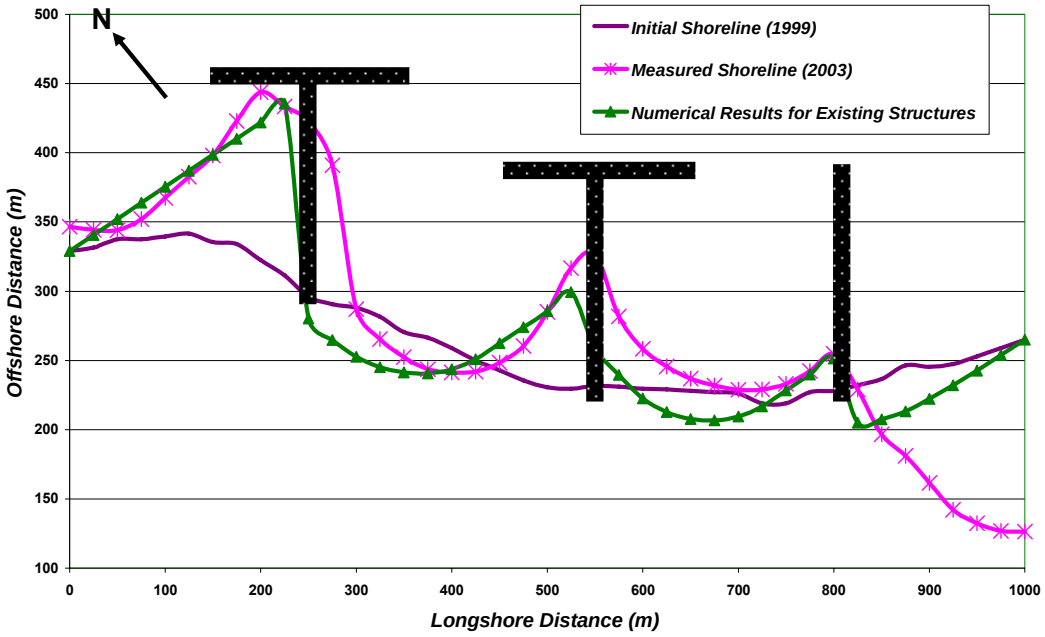

Figure 6.4 *The numerical model results vs. field measurements*

After validating the model with this case study, the shoreline patterns are investigated what if 2 offshore breakwaters had been constructed instead of the existing Y-groins for the same wave data and beach characteristics input. Firstly, the offshore breakwaters are placed in the same locations of the offshore breakwater sections of T-groins but their shore connecting sections are taken out. The results of the numerical results can be viewed comparatively with the field measurements and the numerical results for existing structures in *Figure 6.5*

Besides a second proposal for the structure configuration can be made such that 2 offshore breakwaters are placed instead of the existing Y-groins and a smaller length offshore breakwater compared to other two breakwaters is placed instead of the existing I-groin at the right end of the beach. However, in this case these three breakwaters are placed nearer to the shore compared to the structures given in *Figure 6.5*, which could decrease the cost of the project as well as the maintenance costs. The results are presented in Figure 6.6.

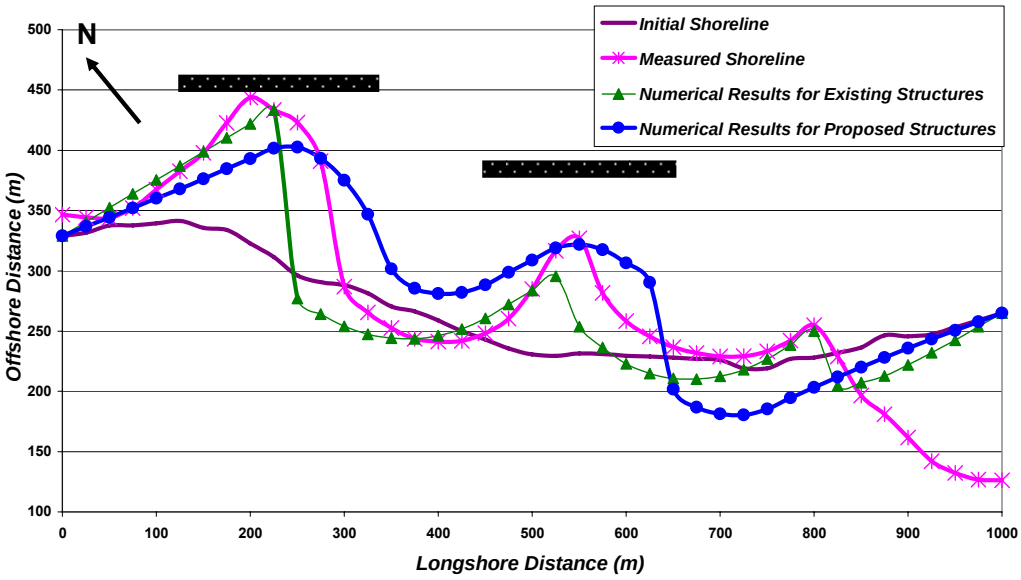

Figure 6.5 *Comparison between the numerical results of the existing structures and the proposed structures (2 offshore breakwaters)*

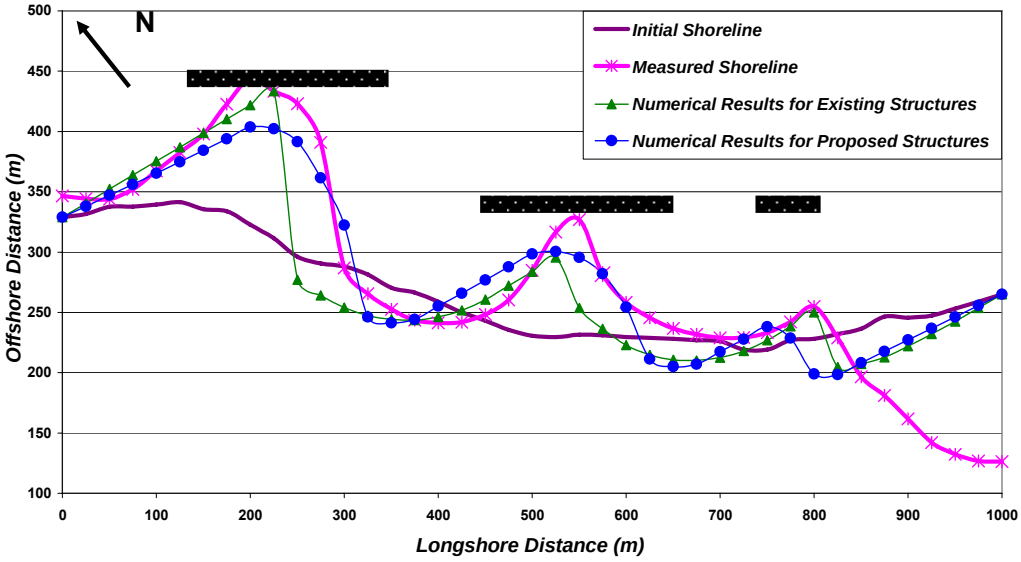

Figure 6.6 *Comparison between the numerical results of the existing structures and the proposed structures (3 offshore breakwaters)*

As it is seen from *Figure 6.5 and Figure 6.6*, the numerical results obtained from the proposed coastal structures (2 offshore breakwaters *in Figure 6.5* and 3 offshore breakwaters in *Figure 6.6*) indicate that using offshore breakwaters instead of Y-groins and I-groins lead to a more balanced shoreline change where erosion and accretion patterns are more uniformly distributed. Offshore breakwaters not only protect the beach behind by reducing wave energy but also they do not completely block the longshore sediment transport rate giving less harm to adjacent beaches compared to other coastal defence structures. Besides offshore breakwaters are more appealing structures from the aesthetical point of view compared to I and T shaped groins since they do not have connection to the shoreline.

CHAPTER 7

CONCLUSION

Shoreline evolution is a complex process with the difficulties and uncertainties inherent in the interaction of wave, current, beach and coastal defence structure parameters. However, within the boundaries of the assumptions and limitations of one-line theory, a numerical model is developed in which groins, offshore breakwaters, T-groins and seawalls or random combination of these structures with arbitrary dimensions can be introduced for predicting shoreline position driven by wind waves.

It is assumed that an unchanged beach profile considered in long term scale, the beach profile moves parallel to itself either onshore (causing erosion) or offshore (leading to accretion), up to a depth of closure, the offshore side of which is free from sediment motion. Governing sand continuity equation in one-line modeling is approached by the explicit scheme finite difference methodology. Depth of closure and depth of longshore sediment transport concepts are clarified.

Wave breaking criteria are comparatively reviewed in order to select the appropriate expressions to be used in the numerical model. The expression of CEM (2003), *Eqn. (3.27)* is selected to be used in the model based on the discussion of slope dependent wave breaker index (γ_b).

Based on the case study for Bafra Delta for which different longshore sediment transport rate expressions are compared with the field measurements, it is seen that shoreline position found by Kamphuis's expression *Eqn. (4.19)* is qualitatively in good agreement with the measured field data which is encouraging for the numerical model. Therefore Kamphuis's (1991) expression is used in the numerical model.

After selecting the appropriate breaking and longshore sediment transport rate relationships to be used in the numerical model, offshore breakwater module of the program in which the morphological changes of shoreline are computed in the lee of a single offshore breakwater or multiple offshore breakwaters. Empirical works of researchers to predict the salient sizes behind offshore breakwaters are reviewed. Wave diffraction patterns behind single offshore breakwaters affecting wave breaking height and breaker angle are defined in the sheltered zone behind the offshore breakwater to be used in the model. Model results of shoreline configurations are compared with the shoreline change given in the literature within the sheltered zone behind the offshore breakwaters.

Multiple offshore breakwater case is also adapted to the numerical model. Wave transmission through the offshore breakwater is inserted into the numerical model and pertinent simulations are presented to test the applicability of these concepts in the numerical model.

Finally a comparative study with the application presented for Bafra Delta where existing Y-groins are replaced by offshore breakwaters. The numerical model results with offshore breakwaters matched well with the expected shoreline changes behind offshore breakwaters. When comparing the shoreline changes obtained from the numerical models for offshore breakwaters with the field measurement for existing 2-Y groins and I-groin, it is seen that using offshore breakwaters leads to a more balanced shoreline where erosion and accretion patterns are more uniformly distributed. This is because offshore breakwaters do not completely block the longshore sediment movement. Besides, from the aesthetical point of view, offshore breakwaters are more appealing coastal defence structures compared to others such as I shaped groin, T shaped groin and seawalls.

Although in Bafra Delta case study, T-groins which are interpreted as a combination of an I-groin and an offshore breakwater resulted in good agreement with the field case proving to validate the model for both offshore breakwaters and groins, in future studies, it is important to compare the model results of

shoreline changes behind a single offshore breakwater with the actual field measurements to calibrate and improve the numerical model.

Also implicit scheme methodology is recommended to use for improving the stability of the numerical program in further studies. A slope dependent breaker depth index γ_b may be used instead of γ_b=0.78. Moreover, longshore gradient of breaking wave height ($\delta H_b / \delta x$) can be implemented into the longshore sediment transport rate formula to enhance the prediction capability of the numerical tool especially within the vicinity of coastal defence structures (Hanson & Kraus, 1991). Reflection process in the vicinity of the structures could also be inserted in the model which also enhances the model capabilities.

REFERENCES

Arı, H.A., (2004), "Kıyı Çizgisinin Sayısal Modellemesi Üzerıne Bir Çalışma; Karaburun Örnegi" M.S.Thesis, YTU, İstanbul (in Turkish).

Bagnold, R.A., (1963), "Mechanics of Marine Sedimentation, in: The Sea, Vol.3 pg.507-528, edited by M.N.Hill, Interscience, NY.

Baykal, C., (2006), "Numerical Modeling of Wave Diffraction in One-Dimensional Shoreline Change Model", M.S.Thesis, METU, Ankara (in print).

Bijker, E.W., (1971), "Longshore Transport Computations", Journal of Waterways, Harbors and Coastal Engineering Division, ASCE, Volume 97, pg.687-701.

Black, K. P., and C. Andrews, (2001a) "Sandy Shoreline Response to Offshore obstacles Part 1: Salient and Tombolo Geometry and Shape", Journal of Coastal Research, Special Issue 29: 82-93.

Black, K.P., (2003), "Numerical Prediction of Salient Formation in The Lee of Offshore Reefs", Proceedings of the 3rd International Surfing Reef Symposium, Raglan, New Zealand,. pg. 196-218.

Bodge, K. R., and Dean, R. G., (1987), "Short-term impoundment of longshore transport" Proceedings of Coastal Sediments '87. ASCE, New York, pg.468-483.

Coastal Engineering Technical Note CETN-III-22 4/84, (1984), "Use Of Segmented Offshore Breakwaters for Beach Erosion Control", U.S. Army Eng. Waterways Experiment Station, CERC.

Coastal Engineering Technical Note CETN-III-43, (1991), "Empirical Methods for The Functional Design of Detached Breakwaters for Shoreline Stabilization", U.S. Army Eng. Waterways Experiment Station, CERC.

Coastal Engineering Manual, (Part II-Chapter 4; Part III-Chapter 2; Part V-Chapter 3), (2003) U.S. Army Corps of Engineers, Coastal Engineering Research Center, U.S.Government Printing Office.

Collins, J. I., (1970), "Probabilities of Breaking Wave Characteristics," Proceedings of the 12th Coastal Engineering Conference, American Society of Civil Engineers, pg. 1993-2004.

Dabees, M.A., Kamphuis J.W., (1998), "ONELINE, A Numerical Model for Shoreline Change", Proc. 26th Int. Conf. On Co. Eng., ASCE, Copenhagen, pg. 2668-2681.

Dabees, M.A., (2000), "Efficient Modeling of Beach Evolution", Ph.D. Thesis, Queen's University, Kingston, Ontario, Canada.

Dabees, M.A., Moore, B.D., Humiston, K.K., (2004), "Enhancement of T-Groin's Design to Improve Downdrift Shoreline Response" Coastal Engineering.

Dean, R.G., (1977), "Equilibrium Beach Profiles, U.S. Atlantic and Gulf Coasts", Tech. Rep. No 12, U. Delaware, Newark.

del Valle, R., Medina, R., and Losada, M. A., (1993), "Dependence of Coefficient K on Grain Size," Technical Note No. 3062, Journal of Waterway, Port, Coastal, and Ocean Engineering, Vol. 119, No. 5, September/October, pg. 568-574.

Ergin, A., (1998), "Coastal Engineering-Lecture Notes", Middle East Technical University, Civil Engineering Department, Ankara.

Galvin, C. J., (1968), "Breaker Type Classification on Three Laboratory Beaches," Journal of Geophysical Research, Vol. 73, No. 12, pp 3651-3659.

Goda, Y., (1985), "Random Seas and Design of Maritime Structures", University of Tokyo Press.

Google Earth, (2006), (http://earth.google.com).

Güler, I., (1997), "Investigation on Protection of Manavgat River Mouth", Yüksel Proje International Co.Inc., Research Project Report.

Güler, I., Ergin, A., and Yalçıner, A.C., (1998), "The Effect of the Use of Wave Data for the Numerical Solution of Shoreline Evolution", Journal of Coastal Research, Special Issue No.26, pg. 195-200.

Hallermeier, R.J., (1978), "Uses for a Calculated Limit Depth to Beach Erosion", Proceedings of the 16th Coastal Engineering Conference, American Society of Civil Engineers, New York, NY, pp.1493-1512.

Hanson, H., (1987), "GENESIS: A Generalized Shoreline Change Numerical Model for Engineering Use", Ph.D. Thesis, University of Lund, Lund, Sweden.

Hanson, H., Kraus, N.C., (1986a), "Seawall Boundary Condition in Numerical Models of Shoreline Evolution", Technical Report CERC-86-3, U.S. Army Engineer Waterways Experiment Station, Vicksburg, MS.

Hanson, H., Kraus, N.C., (1991), "Numerical Simulation of Shoreline Change at Lorain, Ohio", Journal of Waterway, Port, Coastal and Ocean Engineering, Volume 117, No.1, pg.1-18.

Hanson, H., Kraus, N.C., (1989), "Genesis: Generalized Model for Simulating Shoreline Change", CERC Report 89-19, U.S. Corps of Eng., Vicksburg.

Hsu, J.R.C., and Silvester, R., (1990), "Accretion Behind Single Offshore Breakwater", Journal of Waterway, Port, Coastal and Ocean Engineering, ASCE, Volume 116, No.3, pg. 362 – 380

Kamphuis, J. W., and Readshaw, J. S., (1978), "A Model Study of Alongshore Sediment Transport Rate", Proceedings, 16th International Coastal Engineering Conference, American Society of Civil Engineers, pg. 1656-1674.

Kamphuis, J.W., Warner P., (1987), "A Comparison of Wave Refraction and Wave Breaking in Numerical and Hydraulic Models of Initially Conical Sand Islands", Proc. Canadian Coastal Conf. Pg. 257-275.

Kamphuis, J.W., (1991), "Alongshore Sediment Transport Rate", Journal of Waterway, Port, Coastal and Ocean Engineering, ASCE, Volume 117, pg.624-640

Kamphuis, J.W., (1993), "Effective Modeling of Coastal Morphology", Proc. 11th Australasian Conf. On Coastal and Ocean Eng., Inst. Of Eng. Of Australia, Sydney, pg. 173-179.

Kamphuis, J.W., (2000), "Introduction to Coastal Engineering and Management", World Scientific, Singapore-New Jersey-London-Canada

Kökpınar, M.A., Darama, Y., Güler, I., (2005), "Physical and Numerical Modeling of Shoreline Evaluation of the Kızılırmak River Mouth, Turkey", Journal of Coastal Research, Volume 21 (in print)

Komar, P. D., Inman, D.L., (1970), "Longshore Sand Transport on Beaches", Journal of Geophysical Research, Vol. 75, No.30, pg.5914-5927

Komar, P. D., (1971), "Nearshore Cell Circulation and the Formation of Giant Cusps," Geol. Soc. Am. Bull., Vol. 81, pg. 2643-50.

Komar, P. D., and Gaughan, M. K, (1973), "Airy Wave Theory and Breaker Height Prediction," Proceedings of the 13th Coastal Engineering Conference, American Society of Civil Engineers, pg. 405-418.

Komar, P.D., (1977), "Beach Sand Transport: Distribution and Total Drift", Journal of Waterway, Port, Coastal and Ocean Division, ASCE, Volume 103(WW2), pg.225-239

Komar, P.D., (1979), "Beach Slope Dependence of Longshore Currents", Journal of Waterway, Port, Coastal and Ocean Division, ASCE, Vol.105, WW4.

Kraus, N.C., Gingerich, K.J., and Rosati, J.D., (1989), "DUCK85 Surf Zone Sand Transport Experiment" Technical Report, CERC-89-5, U.S.Army Engineer Waterways Experiment Station, Vicksburg, MS.

Le Mehaute, B., Koh, R.C.Y., (1967), "On the Breaking Waves Arriving at an Angle to the Shore", Journal of Hydraulic Research Vol. 5, No. 1, pg. 7-88.

Leont'yev, I.O., (1999), "Modeling of Morphological Changes due to Coastal Structures", Coastal Engineering 38 Pg.143–166.

McCormick, M.E., (1993), "Equilibrium Shoreline Response to Breakwaters", Journal of Waterway, Port, Coastal and Ocean Engineering, ASCE, Volume 119, No.6, pg.657-670.

McCowan, J. (1891), "On the Solitary Wave," Philosophical Magazine, 5th Series, Vol. 36, pg. 430-437.

Miche, R., (1944), "Mouvemments Ondulatiores de la Mer en Profondeur Constante ou Decroissante", Annales des Ponts et Chaussees, Seiries 3, Issue 363, pg. 25-78, 131-164, 270-292, and 369-406.

Ming, D., Chiew Y.M., (2000), “Shoreline Changes behind Detached Breakwater”, Journal of Waterway, Port, Coastal and Ocean Engineering, Vol.126, No. 2, pg.63-70.

Munk, W.H., (1949), “The Solitary Wave Theory and its Application to Surf Problems”, Symposium on Gravity Waves, Circular No.521, National Bureau of Standards, Washington, D.C., pg. 376-462.

Pelnard-Considere, R., (1956), “Essai de Theorie de l’Evolution des Forms de Rivage en Plage de Sable et de Galets”,4th Journees de l’Hydraulique, Les Energies de la Mer, Question III, Rapport No.1, pg. 289-298.

Perlin, M., Dean, R.G., (1983), “A Numerical Model to Simulate Sediment Transport in the Vicinity of Coastal Structures”, Report MR-83-10, U.S Army Corps of Eng.

Schoones, J.S., Theron, A.K., (1993), “Review of the Field Data-Base for Longshore Sediment Transport”, Coastal Engineering, Vol.19, pg. 1-25.

Seiji, M., Uda, T., and Tanaka, S., (1987), "Statistical Study on the Effect and Stability of Detached Breakwaters", Coastal Engineering in Japan, Vol. 30, No. 1, pp 131-141.

Shore Protection Manual (SPM), (1984), U.S.Government Printing Office, Washington D.C.

Smith, E. R., Ebersole, B. A., Wang P., (2004), “Dependence of Total Longshore Sediment Transport Rates on Incident Wave Parameters and Breaker Type”, U.S Army Corps of Eng. ERDC/CHL CHETN-IV-62.

Suh, K., and Dalrymple, R.A., (1987), “Offshore Breakwaters in Laboratory and Field”, Journal of Waterway, Port, Coastal and Ocean engineering, Volume 113, No.2, pg. 105 - 121

Şafak, (2006), "Numerical Modeling Of Wind Wave Induced Longshore Sediment Transport", M.S.Thesis, METU, Ankara (in print).

Van Rijn, L.C., (2000), "Hydrodynamics, Sediment Dynamics and Morphodynamics during Storm Events in 1998 in the nearshore Zone of Egmond, The Netherlands", Report Z2897. Delft Hydraulics, Delft, the Netherlands.

Van Rijn, L.C., (2002), "Longshore Sediment Transport", Report Z3054.20 Delft Hydraulics, Delft, the Netherlands.

Wamsley T., Hanson, H., Kraus, N. C., (2002), "Wave Transmission at Detached Breakwaters for Shoreline Response Modeling ", U.S Army Corps of Eng., ERDC/CHL CHET-II.

Wang P., Ebersole, B. A., Smith, E. R, (2002), "Longshore Sand Transport – Initial Results from Large-Scale Sediment Transport Facility", U.S Army Corps of Eng. ERDC/CHL CHETN-II-46.

Weggel, J. R., (1972), "Maximum Breaker Height," Journal of the Waterways, Harbors and Coastal Engineering Division, Vol. 98, No. WW4, pg. 529-548.

APPENDIX A

NUMERICAL MODEL STRUCTURE

There are three significant inputs in the numerical model which are the initial shoreline, wave climate input and coastal structure configurations.

Initial shoreline may be an irregular or initially straight shoreline.

Wave climate input is given to the program in an input file in which a single row includes values of significant wave height ($H_{s,0}$) in meters, corresponding wave period (T) in seconds, occurrence frequency in hours and the deep water wave angle (α_0) in degrees, respectively. If there are more than one direction, number of rows is entered in the input file such that they are equal to the number of directions from which the shoreline is subject to wave action. For repeating the input file, in the program you enter the number of years / repetitions which allow you to run the same input data several times.

Arbitrary structure configurations whose dimensions are given randomly are interpreted by the numerical program. For example, for the offshore case herein, the numerical model will require the number of offshore structures, the location of each offshore structure, the length of each offshore structure, the offshore distance of each offshore structure and the transmission coefficient of offshore structure. Input manner for other structures are similar. For groins, the number of groins, the location of each groin, the length of each groin and the permeability of each groin are required.

In *Figure A.1*, the model flowchart is presented below.

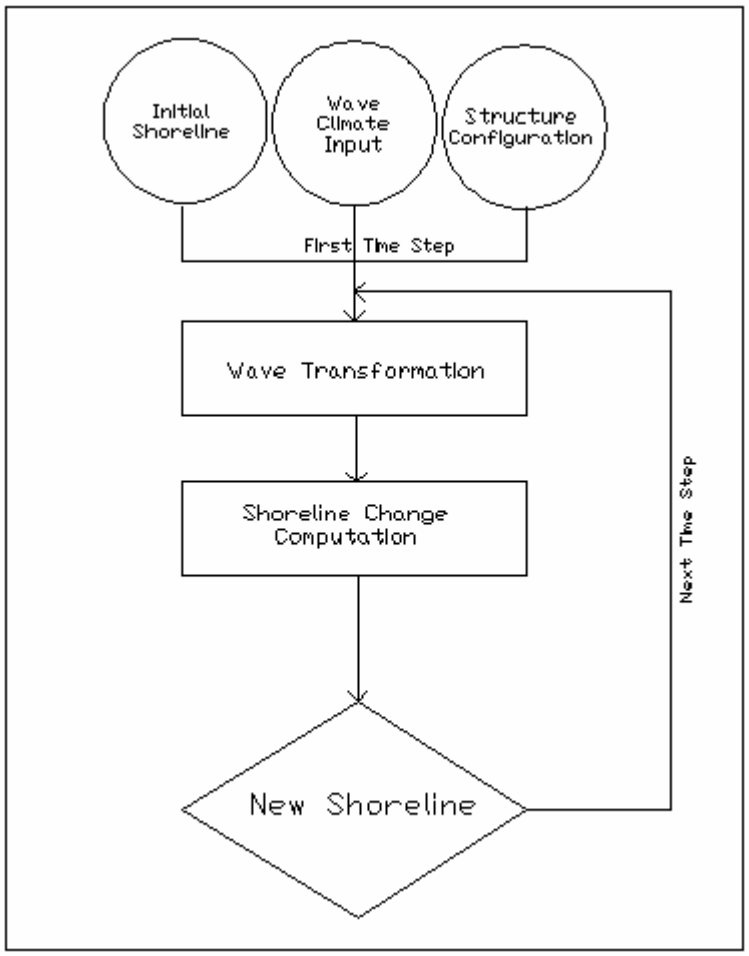

Figure A.1 *Model flowchart*